



# 1 Geophysical downhole logging analysis within the shallow depth ICDP 2 STAR drilling project (Central Italy)

3 Paola Montone<sup>1</sup> \*, Simona Pierdominici<sup>2</sup>, M. Teresa Mariucci<sup>1</sup>, Francesco Mirabella<sup>3</sup>, Marco Urbani<sup>3</sup>,  
4 Assel Akimbekova<sup>3</sup>, Lauro Chiaraluce<sup>1</sup>, Wade Johnson<sup>4</sup> and Massimiliano Rinaldo Barchi<sup>3</sup>

5 <sup>1</sup>Istituto Nazionale di Geofisica e Vulcanologia, Roma, 00143, Italy

6 <sup>2</sup>GFZ, German Research Centre for Geosciences, Telegrafenberg, 14473, Potsdam, Germany

7 <sup>3</sup>Dipartimento di Fisica e Geologia, Università degli Studi di Perugia, Perugia, 06123, Italy (Member of CRUST - Centro  
8 interUniversitario per l'analisi SismoTettonica tridimensionale con applicazioni territoriali)

9 <sup>4</sup>EarthScope Consortium, Boulder, CO, 80301, USA

10 *Correspondence to:* Paola Montone ([paola.montone@ingv.it](mailto:paola.montone@ingv.it))

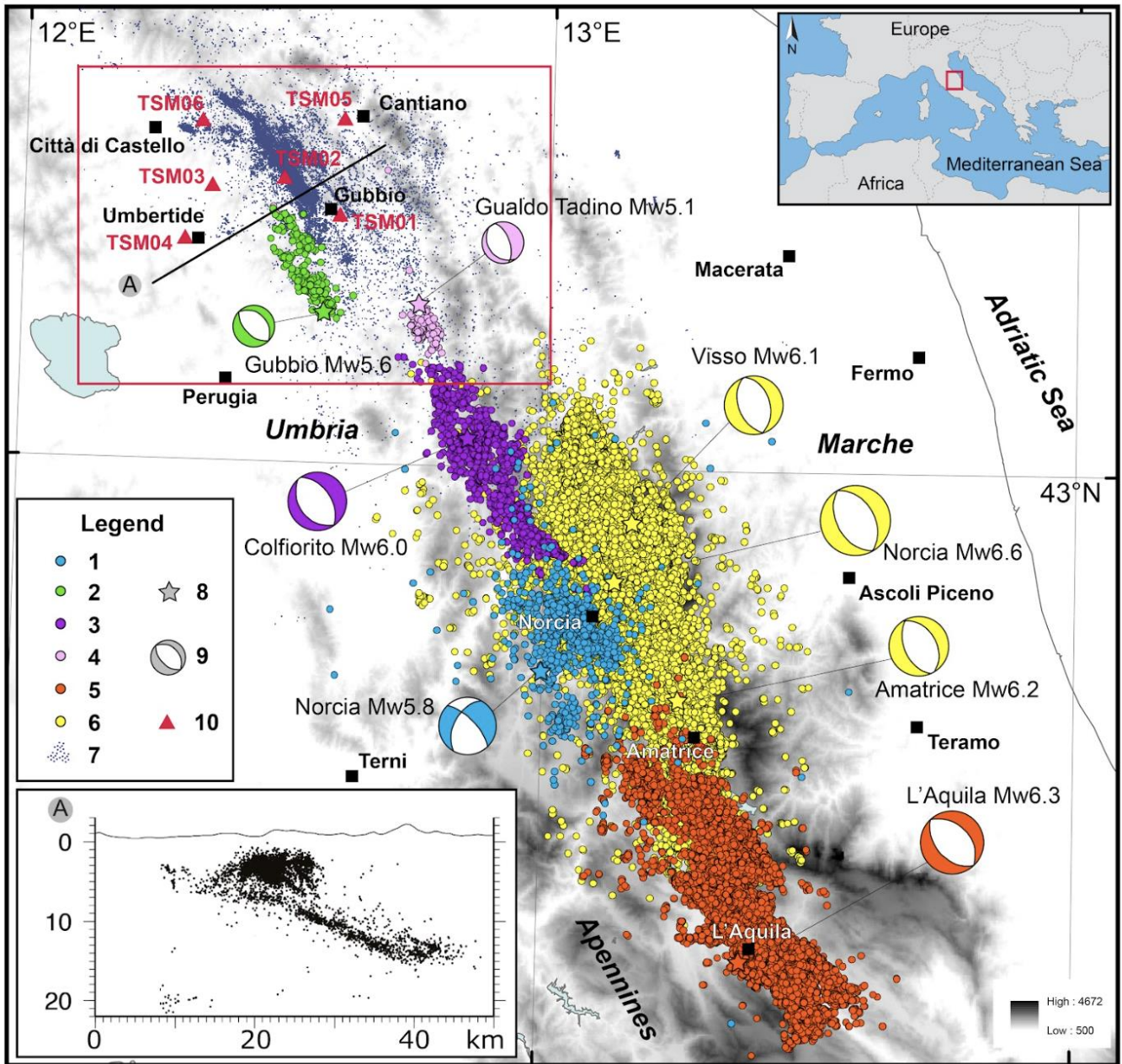
11 **Abstract.** The ICDP STAR drilling project aims to study the seismic and aseismic fault slip behaviour of the active low-angle  
12 Alto Tiberina normal Fault (ATF) in the Northern Apennines, Central Italy, drilling and instrumenting six shallow boreholes  
13 with seismometers and strainmeters. During the STAR field work, a geophysical downhole logging campaign was carried on  
14 defining the optimal target depth for instrument deployment and formation rock characterization. In particular, the main  
15 objectives of this study were to define in situ physical properties of the rocks and the tectonic discontinuity geometry along  
16 the boreholes. The downhole logging data provide new findings and knowledge especially with regards to the physical  
17 properties such as resistivity, gamma ray and wave velocity. The collected parameters were compared to the results of literature  
18 data collected in similar lithologies, as well as with the results of logging performed in deeper wells drilled for commercial  
19 purposes. The physical properties of the Mesozoic-Early Tertiary calcareous formations show low Gamma Ray values and  
20 high compressional ( $V_p$ ) and shear wave ( $V_s$ ) velocities (up to 5.3 km/s and 2.9 km/s, respectively), whereas the overlying  
21 clay-rich Late Tertiary formations exhibit high Gamma Ray and low resistivity and relatively low  $V_p$  and  $V_s$  values (up to 3.5  
22 km/s and 2.0 km/s, respectively). The results obtained from the analysis of the orientations of the tectonic structures, measured  
23 along the six boreholes, show a good agreement with the orientations of the present-day extensional stress field, NE-SW  
24 oriented. Our study allowed to bridge the gap between the physical properties obtained from literature data and those obtained  
25 from the deep wells measurements, representing a possible case history for future projects. These new data will contribute to  
26 the advancement of knowledge of the physical properties of the rocks at shallow depths, typically overlooked.

27  
28



29 **1 Introduction**

30 The aim of the STAR drilling project (A Strainmeter Array Along the Alto Tiberina Fault System) is to study seismic and  
31 aseismic slip on active high- and low angle seismogenic normal faults (Chiaraluce et al., 2023) in Central Italy, an area affected  
32 by seismic events with magnitude up to Mw 6.6 (Fig. 1). The STAR drilling project is an international effort contributing to  
33 the infrastructural implementation of the Alto Tiberina Near Fault Observatory (TABOO-NFO) (Chiaraluce et al., 2014a,  
34 2014b; Chiaraluce et al., 2022), a long-term research infrastructure mapped by the EPOS initiative as one of the European  
35 Solid Earth Science facilities providing open access data to the international community (<http://www.epos-eu.org>). STAR is  
36 one of the International Continental Scientific Drilling Program projects with a primary focus on long-term borehole  
37 monitoring of fault-zone deformation (e.g., Bohnhoff et al., 2017; Fischer et al., 2022).



38

39 **Figure 1: Seismicity in the study area and main seismic sequences in central Italy in the last 45 years. Legend: From 1**  
 40 **to 6:** 1- Norcia 1979 (Deschamps et al., 1984); 2- Gubbio 1984 (Haessler et al., 1988); 3- Colfiorito 1997 (Chiaraluce et

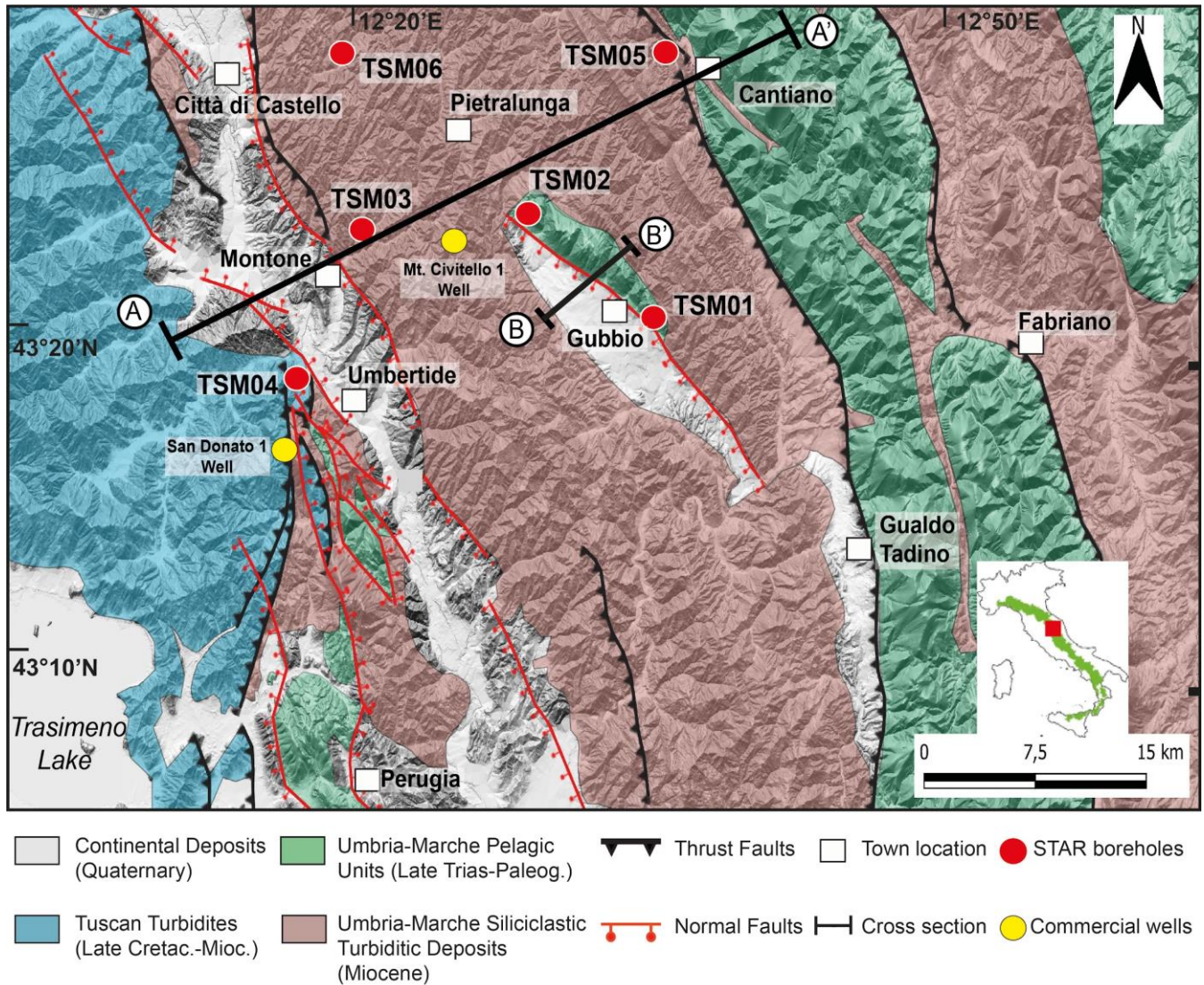
41  
42  
43  
44  
45



46

47 To improve the comprehension of the processes controlling fault mechanics and earthquake generation, the STAR drilling  
48 project installed short period (2Hz) seismometers (three-component borehole geophones) and strainmeters (Gladwin Tensor  
49 Strainmeters, GTSM) in six shallow boreholes (maximum depth 160 m) purpose-drilled. The seismometers were installed to  
50 monitor and record seismicity of the low-angle Alto Tiberina normal Fault (ATF) and its main antithetic splay, the Gubbio  
51 normal fault (Mirabella et al., 2004; Caricchi et al., 2015) (Fig. 2). Borehole strainmeters were deployed because they are the  
52 only instruments able to measure small creep events, as demonstrated in similar experiments focused on other faults, such as  
53 the creeping section of the strike-slip San Andreas fault near Parkfield (Langbein et al., 2006). Seismic and strain observations  
54 from the STAR boreholes monitoring will be integrated with regional observations on active seismicity, on deep crustal  
55 structure and on the present-day stress field.

56 The six 80-160 m shallow monitoring boreholes, named TSM1-6, (see locations in Figure 1) were drilled surrounding the  
57 creeping portion of the ATF in two phases: during the Fall of 2021 and Spring of 2022. The STAR drilling operations were  
58 supported by the acquisition in all the boreholes of a wide set of geophysical logs including: optical (OBI), acoustic (ABI),  
59 caliper (CAL), gamma ray (GR), fluid temperature conductivity (FTC), sonic (FWS), resistivity and spontaneous potential  
60 (ELOG) logs. The borehole geophysical measurement purposes for the STAR drilling project were twofold: firstly, to  
61 characterise the physical properties of the rock formation in the subsurface and, secondly, to identify an intact and competent  
62 fracture-free interval in each borehole in which to deploy the strainmeter and seismometer. After the completion, each borehole  
63 was instrumented and ready for data acquisition (Chiaraluce et al., 2023).



64

65 **Figure 2: Geological setting of the study area. The location of the six STAR boreholes (red circles) drilled in Fall 2021 (TSM01, 02,**  
66 **and 03) and in Summer 2022 (TSM04, 05, and 06), and two deep commercial boreholes (yellow circles), San Donato 1 and Mt.**  
67 **Civitello 1, are displayed. Modified from (Mirabella et al., 2011). The geological cross-sections A-A' and B-B' are in Fig. 3.**

68

69 The objective of this paper is to provide a critical overview of the physical properties of the in-situ rock formations and their  
70 fracture characteristics based on analysis and interpretation of downhole logging data. Particular attention was paid to optical  
71 and acoustic image logs with the aim of identifying intact rock and structural discontinuities. In fractured rock masses,  
72 discontinuities have significant control over the rock mass behaviour. Mapping at depth the fractures and their geometry helped  
73 us identify optimal intervals to host seismometers and strainmeters. In order to work properly and obtain reliable data, these



74 instruments must have a perfect coupling with the rock mass: therefore, borehole seismic installations have to take into account  
75 the borehole diameter and tilt, temperature profile, lithology and fracture distribution.

76 In this paper, after a brief description of the seismicity of central Italy and a geological and tectonic overview of the area where  
77 the boreholes are located, we describe the main results of the operated logging. Geophysical downhole measurements provide  
78 a contribution to better define the physical properties of the Umbria-Marche carbonate multilayer (mainly limestones and  
79 marls) and of the overlying turbidites, cropping out in this area. These results are then compared with the analogue  
80 measurements, acquired in much deeper boreholes, drilled in the same region for hydrocarbon exploration purposes, as well  
81 as with the available, recently acquired laboratory measurements (e.g. De Paola et al., 2009; Smeraglia et al., 2014; Trippetta  
82 et al., 2010, 2021) giving food for thought about the effects of the confining pressure on the physical parameters of the rocks.  
83 In particular, the results related to the P-wave velocities obtained from the sonic log readings along the six STAR boreholes  
84 have been compared with the previous results related to the same geological formations (e.g. Barchi et al., 1998; Diaferia et  
85 al., 2006; Bigi et al., 2011; Mirabella et al., 2011; Scisciani et al., 2014; Porreca et al., 2018; Montone and Mariucci, 2020;  
86 Trippetta et al., 2021). From the geophysical log analysis, we have defined and characterised several planar discontinuities  
87 along each borehole, related either to primary (bedding) or to secondary (tectonic) structures (fault and/or fractures). The  
88 orientations of the tectonic structures, recognized along the boreholes, have been considered together with other available data  
89 and compared with the present-day stress field.

90 Summarising, our paper aims to bridge the gap between the physical properties obtained from literature data (e.g. laboratory  
91 analyses) on outcrop samples and those obtained from the wellbore measurements of oil and gas companies (such as AGIP,  
92 ENI; <https://www.videpi.com/videpi/pozzi/consultabili.asp>), which investigate significantly greater depths. The new data of  
93 this study will contribute to the advancement of knowledge of the physical properties of the rock masses at relatively shallow  
94 depths (0-200 m), typically overlooked. Overall, also considering the results obtained in the analysis and interpretation of the  
95 data in this study, the outcomes from the STAR drilling project will provide a better understanding of the behaviour of the  
96 main active faults, addressing fundamental questions about the relationship between creep, slow slip, dynamic earthquake  
97 rupture, and tectonic faulting (Chiaraluca et al., 2023).

98

## 99 **2 Seismotectonic and geological framework of the area**

100 Seismicity in Central Italy is mainly characterised by shallow crustal earthquakes (5–15 km depth) localised along the  
101 Apennine belt with maximum magnitudes of about 6.6 (Chiaraluca et al., 2017a; Chiarabba et al., 2005). Earthquake focal  
102 mechanisms show a prevalent normal faulting regime, with a NE–SW striking extension, consistent with other data  
103 characterising the active stress field in this area, such as breakouts and active faults (Mariucci and Montone, 2024).

104 In the last 45 years, Central Italy has experienced several crustal normal-faulting earthquakes (Fig. 1) causing surface faulting  
105 as well, visible fractures and significant damage (Cinti et al., 1999; Barchi and Mirabella, 2009; Boncio et al., 2010; Emergeo



106 working Group, 2010; Pizzi et al., 2017; Villani et al., 2018; Barchi and Collettini, 2019). The most significant earthquakes  
107 occurred in the past, with a moment magnitude greater than 5.5 (Fig. 1), are the Mw 5.8 Norcia in 1979, the Mw 5.6 Gubbio  
108 in 1984 and the seismic sequence of Colfiorito-Gualdo Tadino in 1997-98, with the largest event Mw 6.0 (Cello et al., 1997;  
109 Amato et al., 1998; Amato and Cocco, 2000; Boncio and Lavecchia, 2000; Ciaccio et al., 2005; Mildon et al., 2016). Finally,  
110 the seismic sequence that began in 2016 in Amatrice (Tinti et al., 2016; Chiaraluce et al., 2017b; Chiarabba et al., 2018)  
111 occurred with three main events (Mw 6.2 in Amatrice, Mw 6.1 in Visso, and Mw 6.6 in Norcia), causing about 300 deaths,  
112 injuries and the destruction of numerous historic centres (Fig. 1).

113 The six boreholes of the STAR drilling project were drilled in the NW part of the actively extending area of the Umbria-  
114 Marche Apennines (Fig. 2), a NE-verging, arc-shaped foreland fold-and-thrust belt, representing the eastern part of the  
115 Northern Apennines of Italy. Within the study area the compressional structures (folds and thrusts) are mostly arc-shaped with  
116 a roughly NNW-SSE trend and were formed in Late Miocene (Tortonian-Messinian age). They affect a pre-orogenic Jurassic-  
117 Paleogene carbonate multilayer (Umbria-Marche succession) (e.g. Cresta et al., 1989), overlain by a thick succession of syn-  
118 orogenic Neogene turbidites, marls and sandstones, deposited in the Northern Apennines foreland basin (e.g. Barchi, 2010).  
119 The compressional structures are cut and displaced by later (Late Pliocene-Quaternary) NW-SE striking normal faults, which  
120 are related to an extensional stress field oriented in a NE-direction, responsible for the present-day seismicity of the region.  
121 The normal faults attitude is consistent with the extensional stress regime inferred from earthquake focal mechanisms and  
122 borehole breakouts (Mariucci et al., 2008; Montone and Mariucci, 2016; Villani et al., 2018).

123 The most prominent normal fault exposed in the study area is the SW-dipping Gubbio fault, down-throwing the western  
124 backlimb of the Gubbio anticline (Fig. 3). The Gubbio fault is antithetic to a major NE-dipping extensional detachment, i.e.,  
125 the ATF (e.g. Mirabella et al., 2011; Lavecchia et al., 2017). The fault dip of less than 30° makes the ATF an unfavourably  
126 oriented geological structure for reactivation with respect to the regional stress field. The ATF and its high-angle antithetic  
127 splays release continuous microseismicity, and rarer moderate sequences, e.g. in 1984 (Haessler et al., 1988) and in 2010-2014  
128 (Marzorati et al., 2014).

129 The stratigraphy of the study area, from top to bottom, can be summarised as follows (Barchi, 2010): i) marine and continental  
130 Plio-Quaternary sediments, mainly clays and sands in different combinations and with different degrees of compaction; ii) a  
131 thick Neogene synorogenic turbidite succession, namely Marnoso-Arenacea Fm. (Miocene), formed of alternated shales and  
132 sandstones, with strong vertical and lateral variability; iii) a hemipelagic marly succession (Schlier, Bisciario and Scaglia  
133 Cinerea Fms.; Eocene -Miocene); iv) a carbonate pelagic sedimentary sequence of the Umbria-Marche domain (Mesozoic-  
134 Paleogene) that includes not only limestone and chert-bearing limestone but also marl and clay (Scaglia Variegata, Scaglia  
135 Rossa, Scaglia Bianca, Marne a Fucoidi and Maiolica Fms.); v) Lower Jurassic massive platform carbonate (Calcere Massiccio  
136 Fm.); vi) Upper Triassic evaporitic succession, consisting of alternated anhydrites and dolostones (Anidriti di Burano Fm.);  
137 vii) Middle Triassic and/or older continental and shallow marine meta-sediments (Verrucano Fm. s.l.).

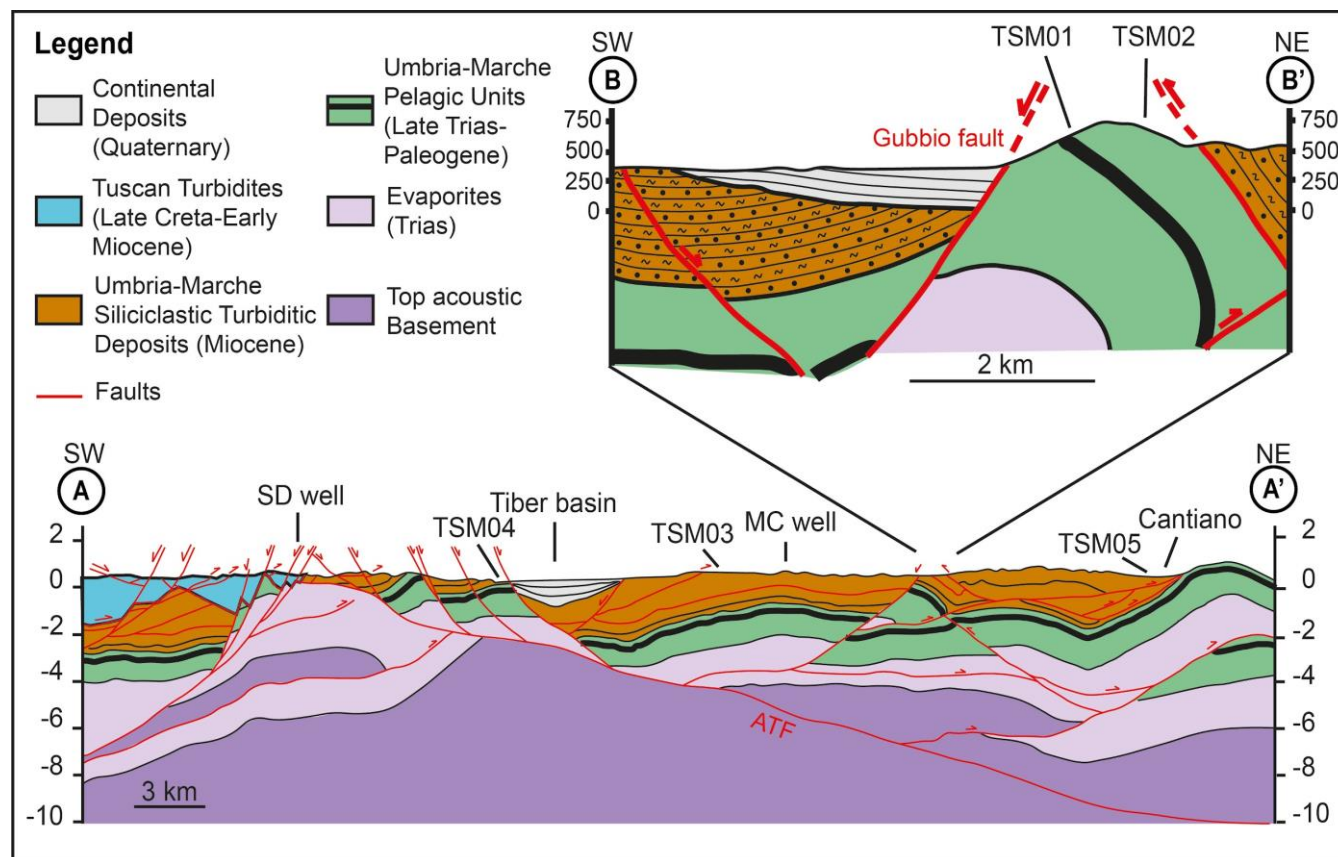


**Figure 3: Geological cross-sections (A-A' and B-B' in Figure 2). The geometry at depth of the main tectonic structures such as the Alto Tiberina low angle normal fault (ATF) and the Gubbio fault (Mirabella et al., 2011) are shown. SD well, San Donato 1 well; MC well, Mt. Civitello 1 well.**

Within the STAR study area (Figures 2 and 3), two deep wells (San Donato 1 and Mt. Civitello 1) were drilled in the past by Italian oil Companies. The wells stratigraphy is schematically reported in previous literature (e.g. Mariucci et al., 2008; Mirabella et al., 2011; Caricchi et al., 2015). The San Donato 1 well (SD), reaching a depth of 4763 m, was drilled by SNIA-BPD in 1983-84 and is located approximately 20 km southwest of the Mt. Civitello 1 well (MC). The SD well is situated very close to the ATF, intersecting it at a depth of 326 m, where the Miocene Marnoso-Arenacea turbidites directly overlie the Triassic evaporitic succession, extending down to a depth of about 3000 m. At greater depth, the well penetrates the metamorphic acoustic basement in tectonic contact with the evaporitic succession (Fig. 3). The MC well, drilled by AGIP in 1988-89, located near the Gubbio fault, reaches a depth of 5600 m. From the surface to a depth of about 1000 m, the well crosses the turbidite succession. Then the well passes through the carbonate Meso-Cenozoic pelagic sequence. From about 2800 m to the bottom at 5600 m, the well crosses the Triassic evaporitic succession.





### 154 **3 Method: downhole logging processing and analysis**

155 The knowledge of the petrophysical properties of the different litho-stratigraphic units is an important aspect to understand  
156 the subsurface. In the lack of coring material, as in the STAR project, data acquisition from downhole logging becomes the  
157 key element in determining the rocks physical characterization (i.e. Rider and Kennedy, 2011). Downhole logging is a method  
158 to gain continuous, in situ high-resolution data of various physical or structural rock parameters collected within a borehole.  
159 For the STAR drilling project, the downhole logging was performed for all six boreholes in order to allow detailed sedimentary  
160 facies assessment and to identify the best location to deploy the strainmeters and seismometers at depth. All six boreholes were  
161 logged by slimhole sondes (for details see Table S1 and text in the Supplementary), and following the standard methods in this  
162 field (Serra, 1984; Ellis and Singer, 2007; Rider and Kennedy, 2011; Schön, 2015; Pierdominici and Kück, 2021). Downhole  
163 measurements were conducted in each borehole after the drilling operations and executed mainly in the open hole (OH)  
164 sections, only GR ran also in the cased section (CH). The following downhole measurements were successfully recorded: total  
165 gamma ray (GR), full waveform sonic (Vp and Vs), temperature (T) and conductivity (COND), three-arm caliper (CAL),  
166 resistivity (RESIST), single point resistance (SPR), and acoustic (ABI) and optical images (OBI). We have summarised the  
167 logging measurements and logged interval for each borehole in Table S1. For the drilling operations, water was used as drilling  
168 fluid allowing to run the OBI. Borehole quality has been determined by vertical and horizontal deviation of the borehole and  
169 the condition of the borehole wall. In order to pursue the objective of the STAR drilling project and for proper use and  
170 performance of the instruments, all six boreholes were drilled within 5° from the vertical. The deviation of each borehole was  
171 then checked as part of the logging program. The boreholes have an inclination of less than 2° except for the borehole TSM06  
172 where the inclination is between 4.3° and 5.1°. Based on i) the smooth borehole wall, ii) log without intervals of large washouts  
173 and iii) internal consistency for several tools (i.e., three different types of borehole diameter measurement), we infer that the  
174 log quality and reliability are very good for almost all sondes over the entire length of each hole.

175 Below, we have summarised the main scientific purpose of each sonde.

176 The total gamma ray log (GR) measures the natural radioactivity of the rock. The GR comes from the radioactive isotopes of  
177 potassium (40K), uranium (238U decay series) and thorium (232Th decay series). Potassium is found primarily in clay  
178 minerals, micas, and potassium feldspar; thorium is commonly associated with clay minerals and volcanic ash layers; uranium  
179 is found in heavy minerals, glauconite and organic rich intervals and may be bound to clay. Relatively high values in GR log  
180 are often associated with the influx of clay and coarser materials, while relatively low GR values generally indicate  
181 sedimentation of biogenic carbonate, organic carbon, or silica (e.g. Rider and Kennedy, 2011). We performed the GR log to  
182 detect layers of clay and to identify changes in lithology. GR was also recorded in drill pipes of all six STAR boreholes,  
183 although the signal appears a bit dampened. In essence, GR log characterises the different lithology crossed by the borehole  
184 allowing to identify layers (thickness and lithotype) through the different clay content.

185 A three-arm caliper (CAL) sonde was used to measure the borehole diameter and to determine how smooth the borehole walls  
186 are. The strainmeter requires relatively smooth walls with no blowouts or fractures.



187 The fluid temperature-conductivity (FTS) measures the temporary temperature and conductivity of the borehole fluid. Both  
188 parameters can show strong variations caused by drilling activities inside the hole but also can detect flow of fluids into or out  
189 of the formation. These logs are good indicators of areas of active flow or open fractures, therefore are used to exclude areas  
190 or intervals with major fractures that would have affected both instrument placement and data quality.

191 The ELOG sonde - including RES and SPR - measures the rock capability to conduct electric currents. The tool provides  
192 resistivity profiles with four different depths of investigation. This measurement provides information about permeability,  
193 porosity, water types and geological formation properties. In particular, in massive rocks with very low matrix  
194 porosity/permeability, the resistivity logs identify fluid filled fracture zones (fracture permeability). So, we ran this logging  
195 sonde for the same reason as the FTS. Only for the TSM01 and TSM02 boreholes the ELOG logs were not acquired.

196 The Full Waveform Sonic (FWS) sonde measures the velocity of sound waves through the rocks, which varies depending on  
197 lithology, rock texture and porosity. The sonic velocity measurement is used for identification of compaction of lithologies,  
198 facies recognition and fracture identification. The velocity has been determined by measuring the travel time of sonic pulses  
199 between transmitters and four receivers. We have reprocessed the raw sonic waveforms to estimate the P and S-wave velocities  
200 using a combination of first arrival trace picking for P and S waves, along with additional semblance analysis.

201 Borehole image sondes provide a continuous oriented high resolution image of the borehole walls. Images collected in the  
202 STAR project have been obtained from acoustic (ABI) and optical (OBI) tools. The latter acquires a true-colour optical image  
203 of the borehole wall, and the acquired data are displayed in one oriented unwrapped image. The sonde operates only in a  
204 transparent drilling fluid like fresh water or air. For TSM04 and TSM06 boreholes no optical image is available due to the  
205 high turbidity of the drilling water. The acoustic image data are visualised as two 360 degrees north-oriented images (travel  
206 time and amplitude) of the borehole wall versus depth. The travel time (TT) provides information about the borehole shape  
207 and the acoustic amplitude (AMPL) depends on the roughness and shape of the borehole wall and its acoustic properties, which  
208 depend on variations with texture, mineralogy, compaction, and fracturing (e.g. Davatzes and Hickman, 2010). These AMPL  
209 and TT images are visualised in colours based on their value range. Here, in the AMPL image, strong contrast (high amplitude,  
210 bright colour) indicates a strong signal and good reflection, and low contrast (low amplitude, dark colour) indicates weak to  
211 missing signals (scattered or absorbed impulse). In the TT image, the bright colours indicate a short time period (fast) for the  
212 impulse to go from the transducer and back to the receiver; the dark colours represent a long time period (slow), which means  
213 widened size of the borehole (e.g. Pierdominici et al., 2020). Each planar discontinuity, such as fracture, fault, bedding, appears  
214 in the images as sine waves (e.g. Davatzes and Hickman, 2010). To obtain a correct geometry of the planar structures (dip  
215 azimuth and dip) the TT and AMPL images have been prior corrected by diameter, inclination and orientation of the borehole.  
216 We have grouped the features in six categories (see Section 4.3): open (in red), filled (in grey), bedding (in green), stylolite (in  
217 turquoise), cherty layer (in dark grey) and weak zones. The acoustic imager tool alone cannot distinguish between open or  
218 closed/filled structures (used here in a general term, i.e., including faults, fractures, and veins). Based on the comparison of  
219 these two images, we might distinguish so-called “open” structures based on their contrast of ultrasonic AMPL and the



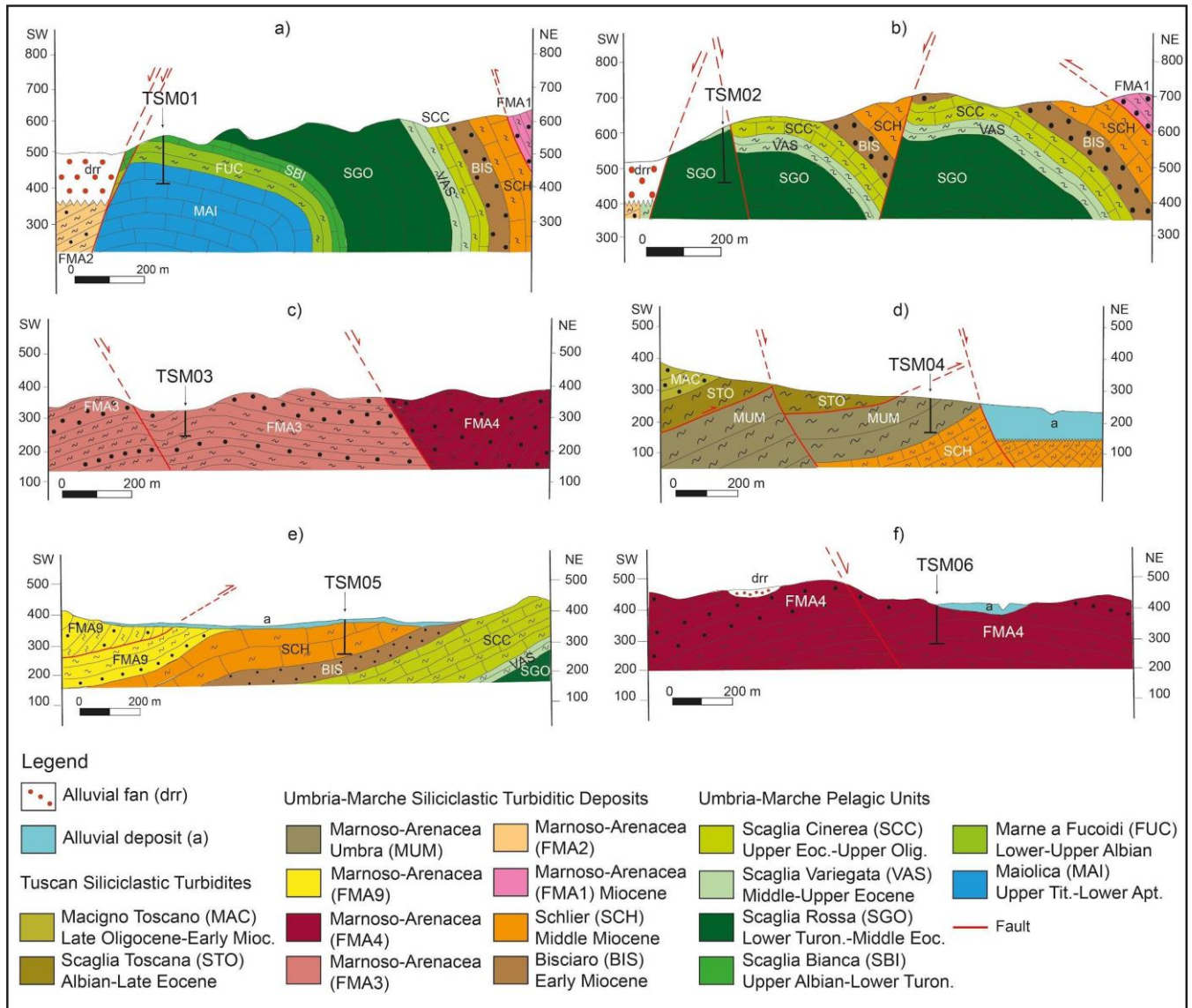
220 corresponding response in the TT. The structures defined as “closed” are visible only in the amplitude image. To enhance the  
221 travel time and amplitude images, static and dynamic (10 cm vertical window) normalizations were applied. Raw, static,  
222 dynamic images display minor differences of each other in the resulting images depending on the scale and variations between  
223 different intervals and features. The displayed images here refer to the static normalisation. The ABI and OBI were also used  
224 to determine the borehole trajectory based on borehole's deviation from vertical (DEVI) and the direction of this deviation  
225 with respect to magnetic north (hole- or drift-azimuth; HAZI). For the installation of strainmeters and seismometers, all STAR  
226 boreholes had to be very close to the vertical. Thus, this type of acquisition played a key role in knowing the condition of the  
227 borehole and decreasing the successful installation of the instruments.

## 228 **4 Data and Results**

### 229 **4.1 Borehole description**

230 The boreholes are located within an area of about 1500 km<sup>2</sup>, centred around the town of Gubbio (Fig. 2). Among the six new  
231 boreholes, TSM01 and TSM02 were drilled across the late Mesozoic-Early Tertiary carbonates, cropping out along the crest  
232 of the Gubbio anticline, which represents the maximum structural culmination of the study area (Fig. 4 a, b). The other  
233 boreholes were drilled in the Tertiary marls and sandstones, cropping out in the northern part of the study area, to the W  
234 (TSM04), N (TSM03 and TSM06) and NE (TSM05) respect to the Gubbio anticline axis (Fig. 4 c, d, e and f).

235 See supplementary files for a lithological detailed description (Supplementary 1).



236

237

238

**Figure 4: Geological cross-sections across the STAR boreholes. Different members of Marnoso-Arenacea Fm. are shown (FMA1, 2, 3, 4, 9 and MUM).**

239

#### 240 4.2 Log results

241

The downhole logging data are described and interpreted to provide new findings and knowledge to complement those obtained from similar rock types sampled in the field outcrops (Fig. 5 and Figs. 6-9).

242

243

Results from the downhole logging analysis are summarised in Table 1 and Table S1 displaying the average values and the related standard deviation. More details are described in Supplementary 2.

244

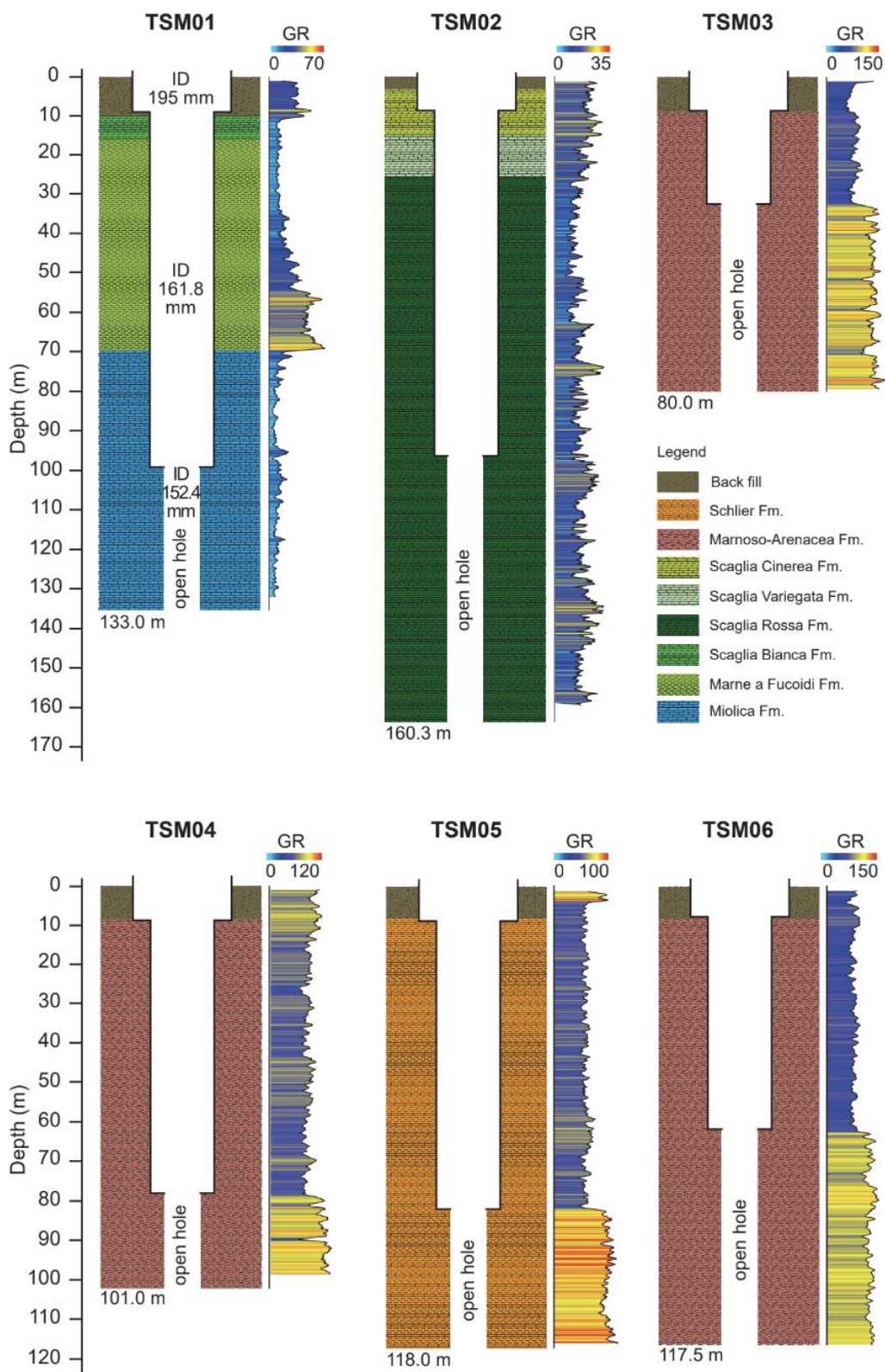


Borehole	ICDP-ID	Depth m		GR cps		Vp m/s	Vs m/s	RES Ωm	SPR Ωm	T °C	COND μS/cm
		CH	OH	CH	OH						
TSM01	5070_1_A	0.0-99.3	99.3-133.0	17.9±13.3	8.4±4.4	5324±371	2885±112	n.d	n.d	12.3±0.6	380.9±39.9
TSM02	5070_2_A	0.0-97.0	97.0-160.3	11.7±5.4	13.4±5.6	4867±184	2505±500	n.d	n.d	14.7±1.3	456.4±61.5
TSM03	5070_3_B	0.0-32.0	32.0-80.0	61.5±12.7	104.2±15.9	3204±168	1800±130	29.2±4.7	104.3±10.4	13.6±0.2	451.6±7.4
TSM04	5070_4_A	0.0-79.3	79.3-101.0	61.5±10.0	85.1±13.2	2972±207	1993±118	8.6±1.0	42.2±4.6	16.2±0.3	694.3±91.7
TSM05	5070_5_A	0.0-82.3	82.3-118.0	48.6±8.7	81.2±9.3	3451±160	1879±148	11.5±3.2	53.4±7.2	16.5±0.7	634.0±8.2
TSM06	5070_6_A	0.0-80.0	80.0-117.5	62.4±9.2	99.7±9.35	3422±306	1896±119	18.2±3.2	76.1±8.9	18.2±0.03	487.3±34.4

**Table 1: Geophysical properties of the rocks for TSM boreholes. GR: gamma ray (count per second); Vp and Vs: P- and S wave velocity, respectively; RES: resistivity; SPR: single point resistance; T: temperature; COND: conductivity; CH: cased hole; OH: open hole.**

245  
246  
247  
248  
249

250 GR log response (open and cased hole) in TSM01 and TSM02 boreholes is generally very low (Fig. 5, Table 1). In TSM01,  
251 the low GR, associated with the limestone Scaglia Bianca Fm., slowly increases in the marly Marne a Fucoidi Fm.,  
252 proportionally to the enrichment of the clay component as well evidenced in the interval between 55.0 m and 66.5 m. The  
253 sharp contact between the Marne a Fucoidi Fm. and the underlying limestone Maiolica Fm. is well indicated by the dramatic  
254 decrease in GR values (from 50 cps of Marne a Fucoidi Fm. to 14 cps of Maiolica Fm.). The open-hole section interests only  
255 the Maiolica Fm. with an average GR value of 8.4 cps. In TSM02, GR records a very low response related to the three pelagic  
256 formations intersected, predominantly consisting of limestones, which are interbedded with sporadic, relatively thin marly  
257 layers as recorded by the increase in GR values (e.g. 73-75 m, 102-104 m, 134-135 m in Scaglia Rossa Fm.). In the TSM03,  
258 TSM04, TSM05 and TSM06 boreholes, GR log shows higher values which vary between 49 cps in TSM05, and 104 cps (open  
259 hole) in TSM03. The GR values are lower in the cased section because the signal is damped by casing. In the open-hole section,  
260 on the other hand, the GR response for all the four boreholes is generally high, displaying relatively uniform cps value ranging  
261 between 81 and 104. Intervals with low GR are few and restricted and likely associated with the presence of fractures and/or  
262 thin sandstone layers. The highest GR values are almost exclusively associated with the marly layers that dominate the  
263 Marnoso-Arenacea Fm. (TSM03, TSM04 and TSM06) and the Schlier Fm. (TSM05).





265 **Figure 5: STAR boreholes with lithostratigraphic profile and gamma-ray log. Each borehole has a conductor casing for the first 9**  
266 **m, followed by a casing and an open-hole section. ID: inner diameters. Only the total gamma (GR, here shown) was also run through**  
267 **the casing, while all other measurements were performed only in the open hole. Seismometers and strainmeters were deployed at**  
268 **the bottom of the open section of each borehole (for details see Fig. S1).**

269  
270 P (Vp) and S (Vs) wave velocities obtained from the full wave sonic log were measured in the open-hole section down to the  
271 bottom of the hole showing a wide range of values between different boreholes: Vp varies between 2972 and 5324 m/s and Vs  
272 between 1800 and 2884 m/s (Table 1; Figs. 6-9). Higher values were recorded along the boreholes that intersected more  
273 competent lithologies, especially limestones as Maiolica Fm. in TSM01 and Scaglia Rossa in TSM02. A significant decrease  
274 of both Vp and Vs was detected at open fractures occurrence. The dynamic Poisson ratio was computed using the specific  
275 formula from shear and compressional sonic logs to compare it to the fracture porosity. As expected, rocks with a low Poisson's  
276 ratio show a higher fracture density (Figs. 6-9).

277 Resistivity was measured in TSM03, TSM04, TSM05 and TSM06 boreholes. The values vary from 9 to 29  $\Omega$ m according to  
278 the response of sonic logs and fracture presence (Table 1); however, with the same lithology the resistivity values vary  
279 following the variations of single point resistance (SPR).

280 Temperature measured in the boreholes (Table 1) is quite constant within a range of 12 to 18°C reflecting the borehole fluid  
281 rather than the “formation temperature”. Due to the shallow investigated depth, the results are not very significant. See Section  
282 3 for details.

283 Conductivity of the drilling fluid is directly proportional to the concentration of dissolved minerals and thus to its salinity: the  
284 highest values (694  $\mu$ S/cm) were found in the TSM04 borehole near the area with intense CO<sub>2</sub> emissions of deep origin (Table  
285 1).

#### 286 4.3 Structure analysis

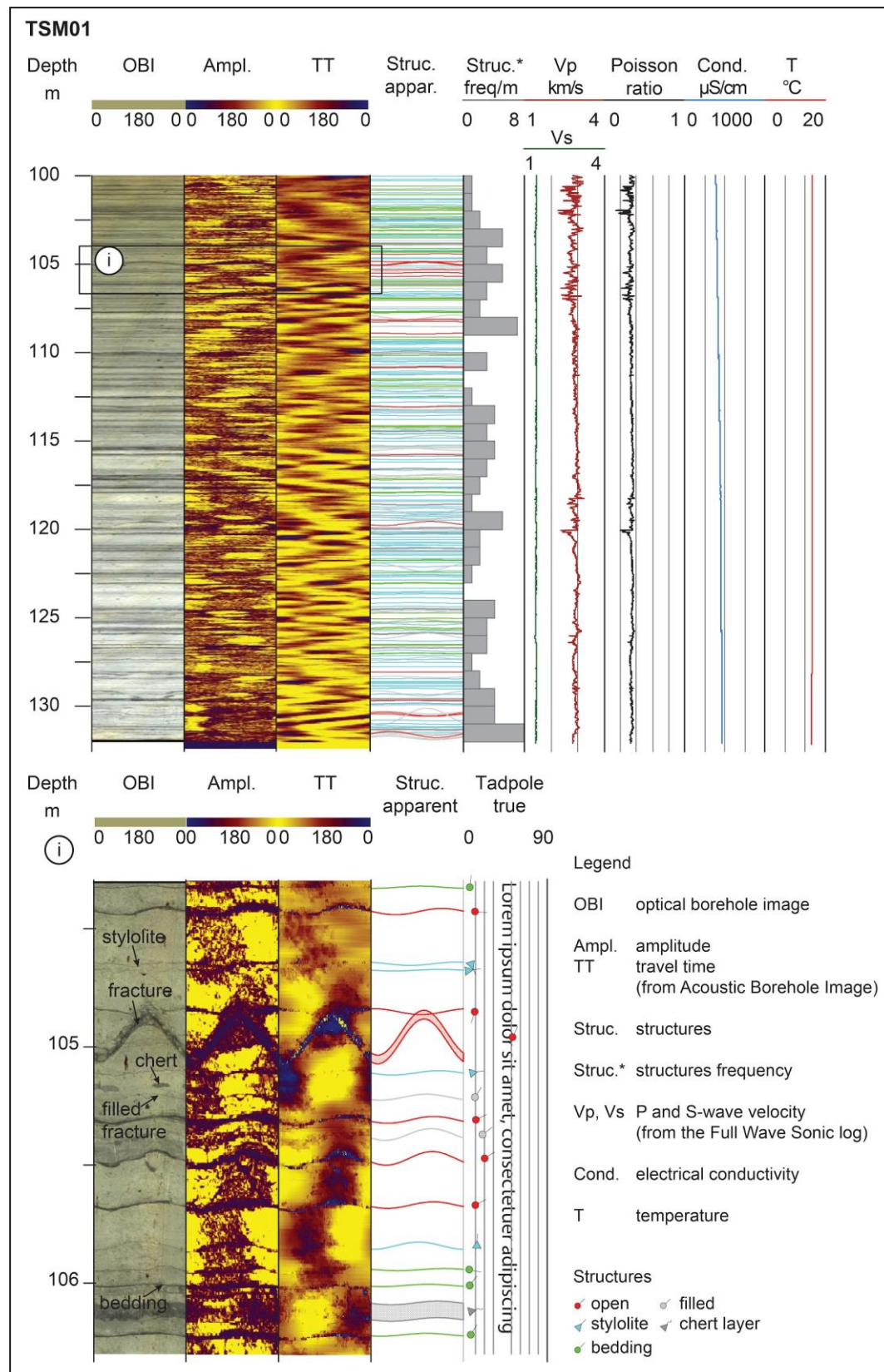
287 In this section we present the analysis of optical and acoustic images performed to identify the main discontinuities along the  
288 boreholes (Figs. 6-9). As mentioned before, we have grouped the features in six categories: open (in red), filled (in grey),  
289 bedding (in green), stylolite (in turquoise), chert layer (in dark grey) and weak zones. The filled and open fractures usually  
290 have a thickness from a few mm up to 1-2 cm. Furthermore, we plotted the main tectonic structures (open and filled fractures  
291 and weak zones) as rose diagrams splitting the data according to their dipping ( $>$  and  $<$  45°).

292 **TSM01.** The analysis of OBI and ABI images allowed us to identify and detect the main discontinuities crossed by the borehole  
293 (Fig. 6). The sub-horizontal discontinuities correspond to bedding planes, while the filled discontinuities can be interpreted as  
294 later-filled fractures or cleavage planes. Moreover, numerous stylolites and chert layers are present within the Maiolica Fm.,  
295 both parallel to bedding. A detail of the main features is shown in the inset of Fig. 6-i. A total of 69 discontinuities (only open  
296 and filled fractures) were recorded along the open-hole section showing a homogeneous distribution along the borehole with  
297 a maximum of 8 structures per metre. The preferential orientation is NW-SE, corresponding to a dip azimuth of N200° (Fig.



298 10). The dip of these planes is generally low (around  $25^\circ$ ), contributing to the azimuthal dispersion of the data. However, some  
299 discontinuities with steeper dips (ranging from  $60^\circ$  to  $80^\circ$ ) are still NW-SE oriented.





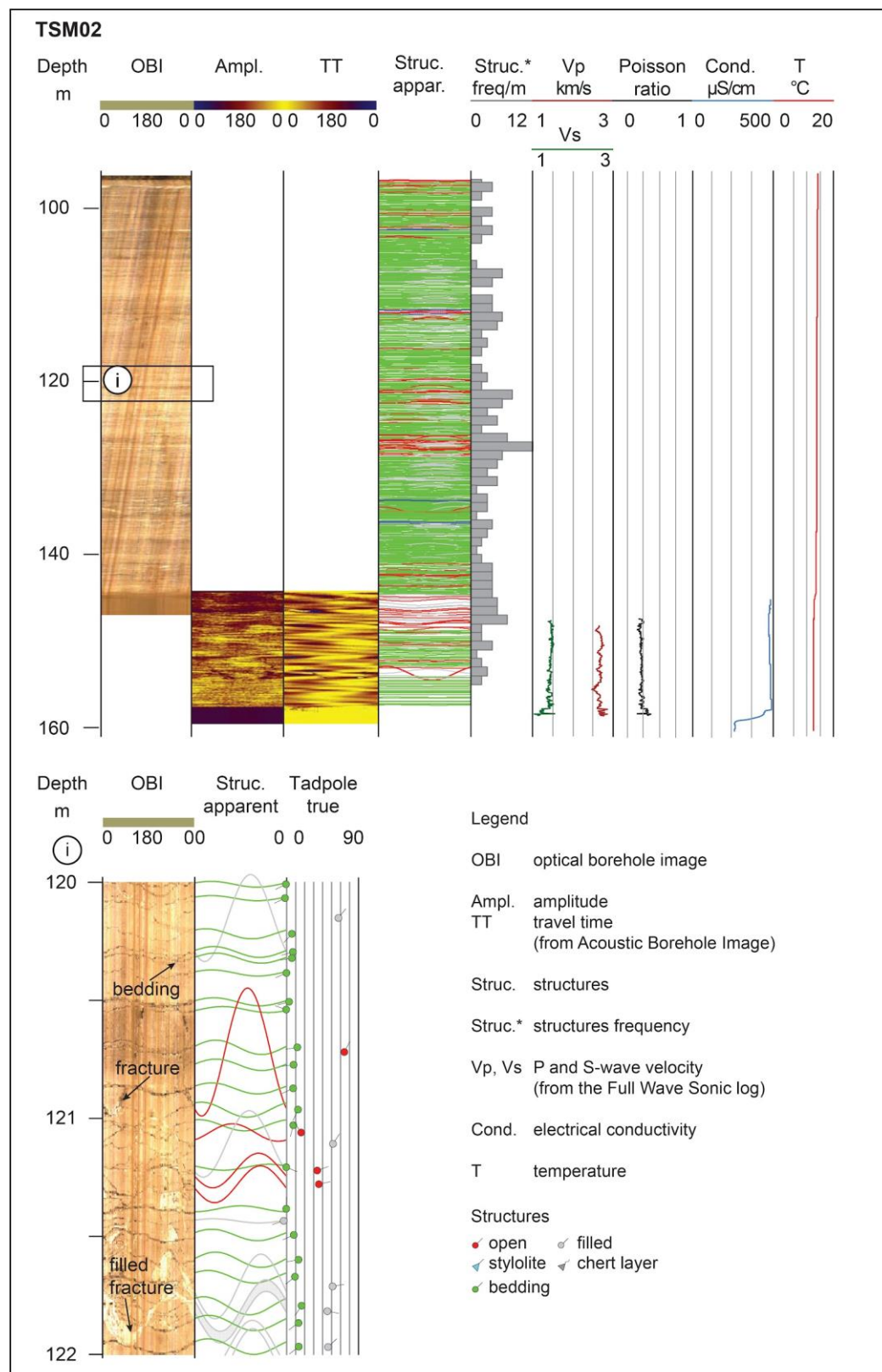


301 **Figure 6: Downhole logging measurements performed along the TSM01 borehole (Maiolica Fm.). At the bottom: a detail of the**  
302 **structures intersected by the borehole.**

303

304 **TSM02.** The OBI and ABI images available for structural analysis investigated two different depth ranges. The OBI was  
305 performed from 96.2 to 147.0 m and the ABI from 144.2 to 159.6 m. The OBI image clearly shows continuous and parallel  
306 layering and especially the interlayering of thin clay layers in the limestone. The Scaglia Rossa Fm. is also affected by  
307 numerous thick filled and open fractures. The analysis of the planar discontinuities identified on both images allowed us to  
308 distinguish bedding planes, filled and open fractures (Fig. 7). The latter two structures (195 counts) revealed a predominant  
309 orientation of NNW-SSE, corresponding to a dip azimuth of  $N204^\circ$  (Fig. 10), with an average structure frequency of 6 per  
310 metre and a high discontinuities concentration around 120 to 125 m (Fig. 7-i). The majority of open and filled fractures have  
311 dipping values higher than  $45^\circ$ , the open ones dipping almost exclusively to NE, and the closed ones to SW (Fig. 10).

312



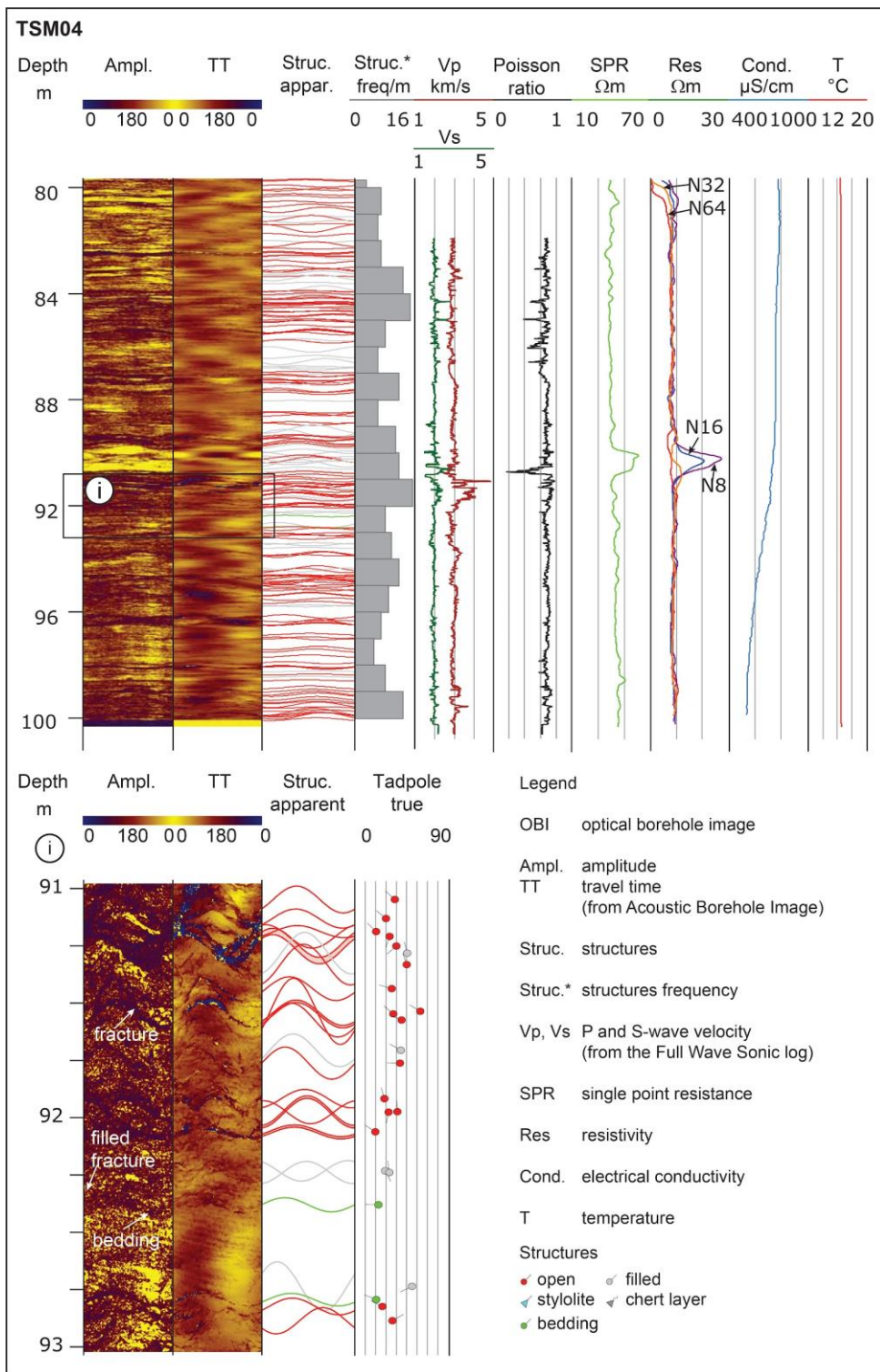


314 **Figure 7: Downhole logging measurements performed along the TSM02 borehole (Scaglia Rossa Fm.). At the bottom: a detail of the**  
315 **structures intersected by the borehole.**

316

317 **TSM03.** The poor quality of the OBI and ABI images made it difficult to perform a successful structural analysis. The unclear  
318 images are related to the high turbidity of the fluid in the borehole due to non-flushing of the borehole prior to acquisition and  
319 the high speed of running the OBI and ABI probes. Only the bedding planes were recognized showing a mean orientation of  
320 NW-SE (dip azimuth of N201°) with a very low dip of 11°. Owing to the low quality of the images, a geological survey was  
321 performed to measure bedding and main tectonic structures directly on the Marnoso-Arenacea outcrop near the drilling site  
322 (Fig. S2). Bedding varies from N204 near the borehole, to N167 and N155, dipping about 5-15°W, consistent with what was  
323 observed from the data analysis along the borehole. The thickness of the sandstone levels of Marnoso-Arenacea Fm. is up to  
324 100-120 cm, while the thickness of the grey marly layers ranges from 1 to 10 cm; they are laminated with cleavage planes sub-  
325 parallel to the bedding. There are fractures and sometimes sub-vertical faults, which are clearly visible in the sandstone layers,  
326 with an average fracture orientation of N050 sub-vertical, N215 sub-vertical faults with extensional displacement, N213  
327 dipping 76°W with left-lateral striae overlapped with oblique striae (pitch 55°, Fig. S2).

328 **TSM04.** The borehole intersected numerous discontinuity planes along the entire length of the measured log (Fig. 8). Although  
329 the log length is approximately only 20 m (79.8 to 100 m), the quality of the ABI images is significantly better compared to  
330 the TSM03 and TSM06 boreholes drilled in the same formation (Marnoso-Arenacea Fm.). The drastic decrease of cloudy fluid  
331 in the borehole is the combined result of wellbore flushing operations before starting log acquisition, and the low running  
332 speed of the ABI probe resulting in a good ABI image quality. 195 discontinuities between filled and open have been detected  
333 on image log with an average orientation of N184 and dipping never exceeding 60° (Fig. 10). In the field, upstream of the  
334 drilling site (Fig. S2), it was possible to measure bedding that is N180 oriented, dipping 25°W related to a small Late  
335 Cretaceous-Early Miocene outcrop of Tuscan turbidites (Fig. 2).

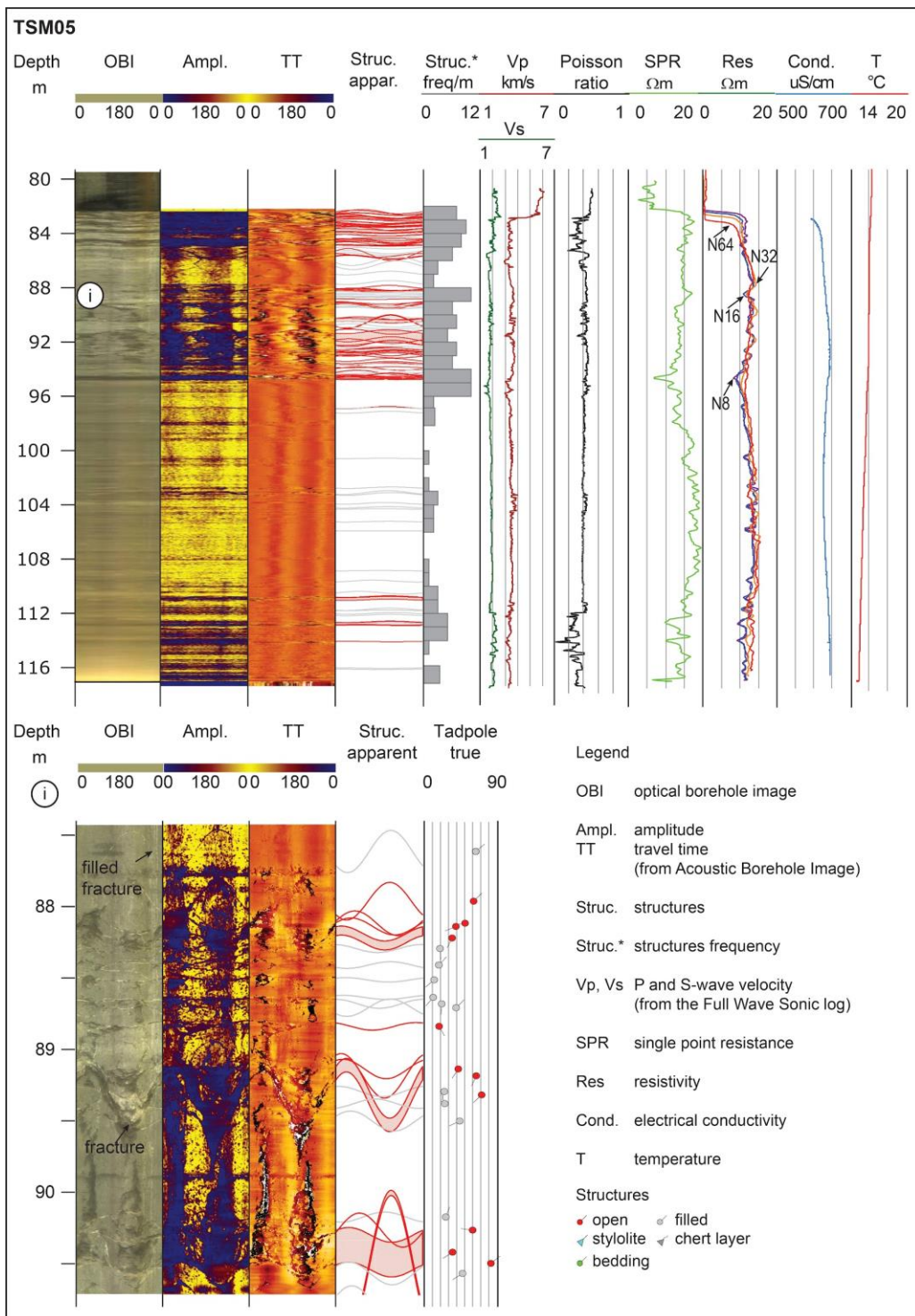




337 **Figure 8: Downhole logging measurements performed along the TSM04 borehole (Marnoso-Arenacea Fm.). At the bottom: a detail**  
338 **of the structures intersected by the borehole.**

339

340 **TSM05.** Analysis on OBI and ABI images allowed to clearly identify tectonic structures such as open and filled structures  
341 (Fig. 9). The bedding planes instead are dubious and difficult to recognize. Discontinuity planes show a spacing quite dense  
342 (12 planes per 1 m) up to 94.8 metres; below, they are very sparse, with sections of up to 3 m without discontinuity probably  
343 also due to the acquisition and to the presence of cloudy drilling fluid in the borehole. From the image analysis a total of 114  
344 planar structures have been identified with very consistent NW-SE orientation (corresponding to a dip azimuth of N219; Fig.  
345 10). From this dataset, we have marked at least 4 different categories of discontinuity according to their dip, the presence or  
346 absence of filling and their aperture. A first category of discontinuities is characterised by dip greater than  $45^\circ$  which is related  
347 to both open and filled fractures. They show planes approximately NW-SE oriented with dip both towards SW and towards  
348 NE. The filled fractures with dip less than  $45^\circ$  show a similar NW-SE trend as well as the open fracture zones including wider  
349 zones (decimetre thicknesses up to 1 m; Fig. 9-i) still have a NW-SE orientation and dips ranging from very low to almost  
350 vertical. The bedding planes are mainly sub-horizontal.



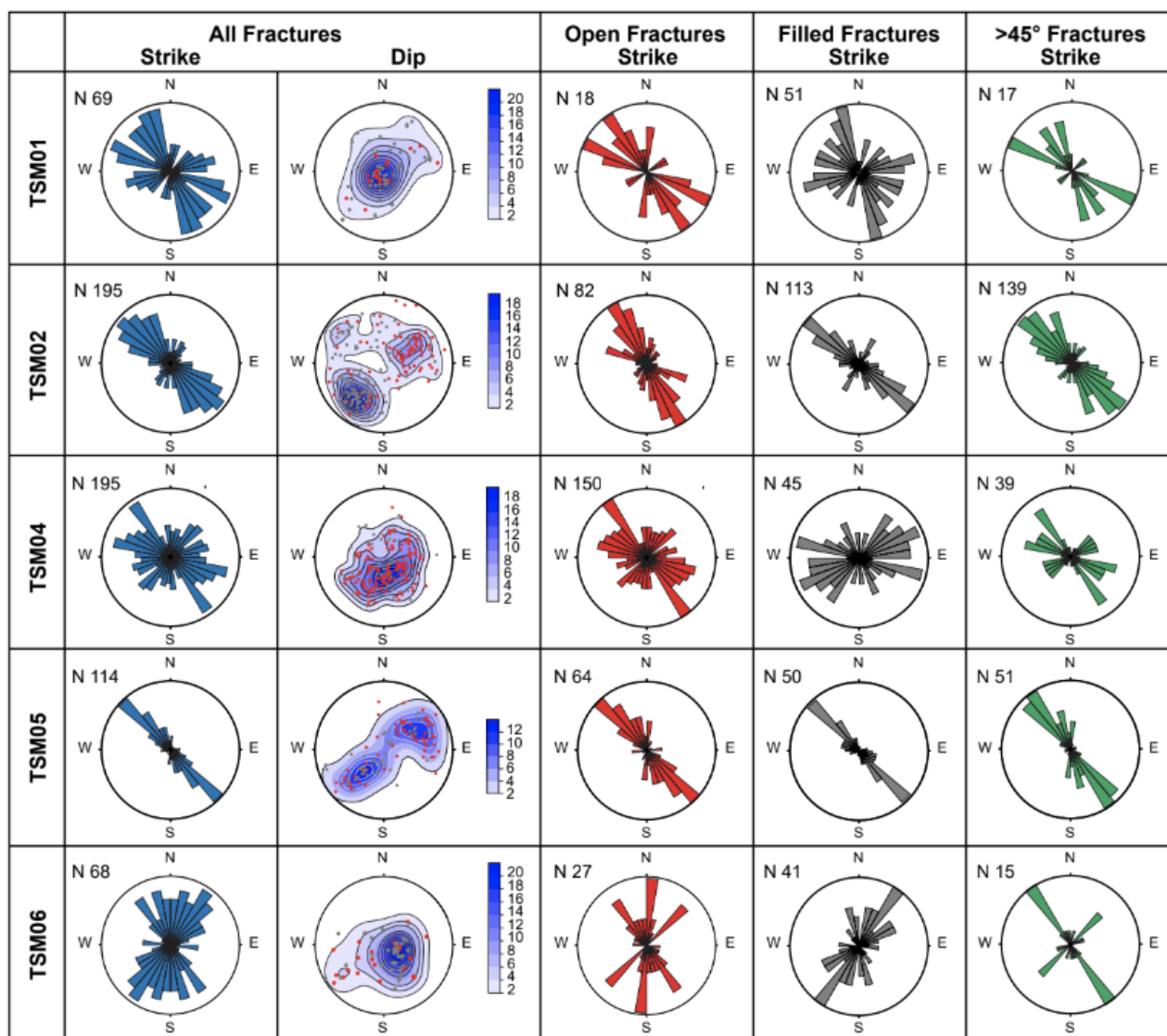


352 **Figure 9: Downhole logging measurements performed along the TSM05 borehole (Schlier Fm.). At the bottom: a detail of the**  
353 **structures intersected by the borehole.**

354

355 **TSM06.** The structural analysis has been performed only on ABI image log allowing to identify 68 planar structures of which  
356 27 open and 41 filled in the Marnoso-Arenacea Fm. (Fig. 10). The planar discontinuities show a prevailing NE-SW orientation,  
357 and dip 20-30°W. There is also a minor NNW-SSE oriented data concentration characterised by steeper dip up to 60°NE. A  
358 weak zone oriented N300 dipping 54°NE with a width of about 21 cm, has also been identified along the TSM06 borehole. In  
359 the field very close to the drilling site, bedding is N190 oriented, dipping 30°W. In the surroundings, low angle bedding planes  
360 are also NW and NE oriented. Fracture planes are N125 oriented, dipping 88°S close to the drill; other high angle tectonic  
361 structures are also E-W and NE-SW (Fig. S2).





362

363

364

365

**Figure 10: Rose diagrams and polar projections related to open and filled structures detected along the STAR boreholes (except TSM03). N: number of structures; DIP: poles of the planes (lower hemisphere) with the contouring (in percentage). The last column represents the fractures dipping >45°.**

366

367

## 5 Discussion and Conclusion

368

369

In the framework of the STAR project, six shallow boreholes were drilled, conducting geophysical downhole logs accurately, aimed to identify the most suitable depth in each borehole for the deployment of seismometers and strainmeters. The results



370 of the seismometer and strainmeter network will require more time to obtain useful information for the project itself, dedicated  
371 to the study of the brittle upper crust, and the structure and behaviour of the Alto Tiberina low-angle seismogenic normal fault,  
372 in particular. This paper pertains solely to the initial phase of the STAR project, specifically focusing on the analysis of  
373 downhole geophysical well logs.

374 Downhole logging was the only way to characterise the borehole section, allowing the physical and structural properties of  
375 each geological formation to be determined, due to the lack of core samples. These in situ measurements are sensitive to  
376 formation properties on a scale that is intermediate between those obtained from literature data analysis performed on core or  
377 outcrop samples and deep geophysical measurements, performed by exploration and production drilling companies.

378

### 379 **5.1 Physical properties**

380 Regarding the calcareous formations of Maiolica and Scaglia Rossa Fms., crossed by the boreholes TSM01 and TSM02,  
381 respectively, the physical properties of these competent rock types are well reflected by the acquired log data (Table 1),  
382 showing low average GR values (less than 18 cps) and relatively high average values of  $V_p$  (5.3 and 4.9 km/s, respectively)  
383 and  $V_s$  (2.9 and 2.5 km/s, respectively). The almost pure limestones of the Maiolica Fm. are characterised by lower GR and  
384 higher  $V_p$  and  $V_s$  values, in comparison with the Scaglia Rossa Fm., where the clay content is significantly higher (up to 20%  
385 in the Tertiary upper portion of the Scaglia Fm., e.g. Arthur and Fischer, 1977).

386 The TSM03, TSM04, TSM05 and TSM06 boreholes were drilled in the marly intervals of the Neogene successions of the  
387 Marnoso-Arenacea Fm. and Schlier Fm. (TSM05). These clay-rich rocks are coherently characterised by high average GR  
388 (between 81 cps in the Schlier Fm. and 104 cps in the Marnoso-Arenacea Fm., TSM03) and low RES (between 9  $\Omega\text{m}$  and 29  
389  $\Omega\text{m}$ ). The measurements include lower values for TSM04 (9  $\Omega\text{m}$ ) and TSM05 (12  $\Omega\text{m}$ ), Marnoso-Arenacea and Schlier  
390 respectively, intermediate values for TSM06 (18  $\Omega\text{m}$ ), and higher values (up to 29  $\Omega\text{m}$ ) for TSM03.

391 In greater detail, the average values are not totally representative of these complex formations, typically consisting of alternated  
392 marls and sandstones: similar suggestion derives from the relatively low  $V_p$  (3.0 to 3.5 km/s) and  $V_s$  (1.8 to ~2.0 km/s) values.  
393 The temperature recorded in the boreholes (Table 1) is rather constant with values between 12°C and 18°C without showing  
394 any significant variations related to e.g. outflow or inflow zones. Unfortunately, the shallow depth of the investigation limits  
395 the significance of the results.

396 We compared our RES results with two deep well data (San Donato 1 and Mt. Civitello 1 wells; <https://www.videpi.com>)  
397 drilled in the same formations and considering the same analysed depth interval, showing similar values between 20  $\Omega\text{m}$  and  
398 30  $\Omega\text{m}$ , for the Marnoso-Arenacea Fm. (Fig. S3). We have also investigated the resistivity of the Schlier Fm. along the Canopo  
399 1 well (<https://www.videpi.com>), although this latter is located far away from the study area, approximately 80 km NNE of  
400 Gubbio. Also in this case the resistivity values, around 7  $\Omega\text{m}$ , are comparable with our data (Fig. S3).



401 Information obtained from the velocity logs are more significant, including all 6 boreholes. We compared the  $V_p$  values  
402 recorded in the six shallow (depth < 0.2 km) STAR boreholes (Table 1) with the data derived from sonic log analysis in much  
403 deeper wells (depth > 4 km), drilled in the same region for industrial purposes, and recently analysed by Montone and Mariucci  
404 (2020) (see also references therein) and Trippetta et al. (2010). These authors report average values between 4 and 4.8 km/s  
405 for Marnoso-Arenacea and Schlier Fms., 5.8 km/s for Scaglia Rossa Fm. and between 5.9 and 6.2 km/s for Maiolica Fm. All  
406 these values are about 30 % higher with respect to our results, but show the same overall trend, where the higher average  $V_p$   
407 values recorded in Maiolica, and the lower ones in the Tertiary marly Fms. This increase in P-wave velocity with depth is  
408 primarily attributed to the increase in density and compaction of the rocks. Due to a different degree of porosity linked to the  
409 different investigated depths and to the pore type, P-wave velocity can significantly change (e.g. Hairabian et al., 2014;  
410 Smeraglia et al., 2014; Trippetta et al., 2021). Moreover, P-wave velocity also depends on factors such as lithology changes,  
411 presence of fractures or faults and also on the different amount of tectonic deformation observed in different structural domains  
412 (Trippetta et al., 2021).

413 Collecting and analysing the velocity data of upper crustal sedimentary rocks is very useful under different aspects. On one  
414 end, these values help in building up and calibrating more accurate, 2D and 3D velocity models, that can be used for improving  
415 the earthquakes localization (e.g. Latorre et al., 2016; Montone and Mariucci, 2023) as well as to constrain depth conversion  
416 of seismic reflection profiles. On the other hand, since the velocity parameters of rocks are strictly related to their rigidity,  
417 velocity values also reflect into their different mechanical behaviour and may ultimately influence earthquake generation and  
418 distribution. In our case, the more competent carbonate formations (i.e. Maiolica and Scaglia Rossa Fms.) are characterised by  
419 systematically higher velocity values with respect to the less competent, clay-rich turbidite formations (i.e. Schlier and  
420 Marnoso-Arenacea Fms.).

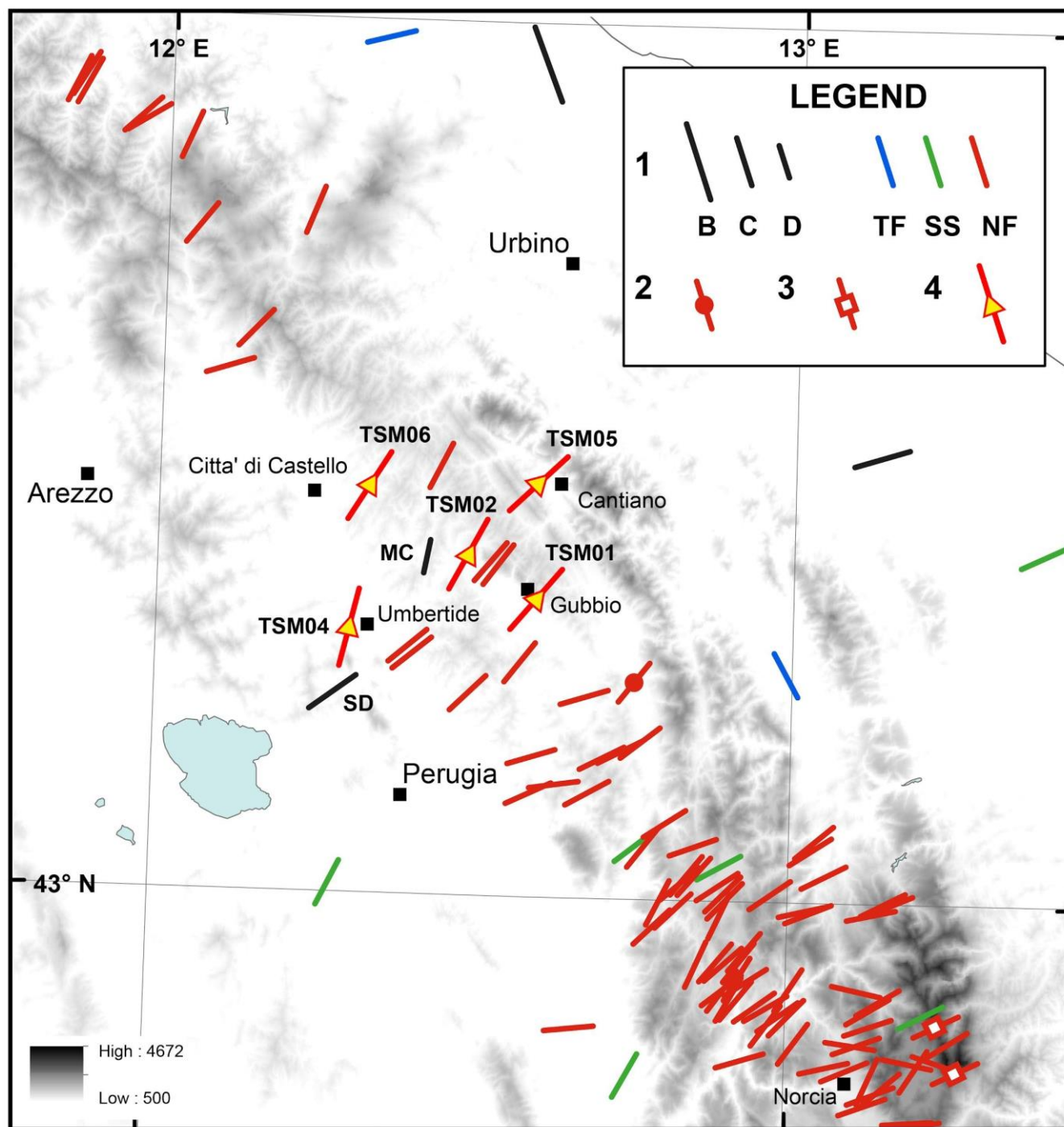
421 In the ATF region, as well as in adjacent areas in the same seismotectonic framework of the Central Apennines, several recent  
422 studies of the relationships between seismicity distribution and upper crustal geological setting have been recently performed,  
423 by plotting accurately relocated seismic sequences on well-calibrated geological subsurface models, based on depth conversion  
424 of seismic reflection profiles (e.g. Latorre et al., 2016; Barchi et al., 2021; Collettini et al., 2022; Chiaraluce et al., 2017b).  
425 These studies coherently indicated that upper crustal seismicity (and the normal faulting earthquake mainshocks, in particular)  
426 are systematically hosted in the high velocity, Mesozoic or Early Tertiary successions, consisting of carbonates, dolostones  
427 and anhydrites, whilst only few, low magnitude events are recorded in the overlying, less competent Neogene turbidites, mainly  
428 consisting of marls and sandstones.

429

## 430 **5.2 Stress Field**



431 As already mentioned, in the STAR study area (Fig. 2) two deep wells (SD and MC) were drilled in the past, reaching a depth  
432 of 4763 and 5600 m, respectively. The SD well is located very close to the ATF, intersecting it at a shallow depth; while the  
433 MC well, approximately 15 km east of the ATF fault, intersects additional tectonic structures. A thorough analysis of borehole  
434 breakout stress data conducted along the two deep wells, allowed to deduce the current stress field orientation (Mariucci et al.,  
435 2008). In the case of the SD well, the borehole breakout results reveal a minimum horizontal stress orientation of  $N055\pm22^\circ$ ;  
436 the MC well exhibits a slightly different stress orientation, with a value of  $N012\pm29^\circ$  (Fig. 11).



437

438

439

440

**Figure 11: Present-day stress field of Central Italy. The minimum horizontal stress orientations inferred both from the >45° dipping fractures detected along the STAR boreholes (bars with yellow triangles) and from the Italian Present-day Stress Indicators database IPSI 1.6 (Mariucci and Montone, 2024) are shown. 1- Stress data scaled by quality (from B to D) and coloured according to tectonic**



441 **regime: black bar is unknown regime (borehole breakout data), blue is thrust faulting, green is strike-slip faulting, red is normal**  
442 **faulting; 2- formal inversion data; 3- fault data; 4- data from TSM boreholes.**

443

444 To interpret the structural data obtained along the STAR boreholes, we have considered i) the shallow depth of the boreholes,  
445 ii) their near-vertical inclination, that strongly underestimates occurrence of near-vertical features (Terzaghi, 1965; Massiot et  
446 al., 2015), and iii) the difficulty in distinguishing fractures from faults in this type of data.

447 Along the STAR boreholes, the main features with a dip angle  $> 45^\circ$  (Fig. 10, column f) show a predominantly NW-SE  
448 orientation and could be interpreted as pre-existing fractures generated in the early phases of the deformation history before  
449 folding (Price, 1966).

450 Considering that the current stress field in the area is primarily due to an extensional regime, with the main compressional  
451 stress,  $\sigma_1$ , vertical and horizontal  $\sigma_3$  NE-SW oriented, the tectonic structures associated with this latter stress field  
452 consequently develop normal faults and high-dip extensional fractures. These  $> 45^\circ$  NW-SE structures, favourably oriented  
453 with respect to the current extensional stress field (Fig. 11), might have been reactivated as extensional fractures. In TSM04  
454 and TSM06 boreholes, for structures with a dip greater than  $45^\circ$  (Fig. 10, column f), another orientation is also observed,  
455 approximately  $90^\circ$  from the previous one. We can assume that both fractures NW-SE and NE-SW oriented are  
456 contemporaneous and linked to the same extensional stress field, primarily guided by a vertical  $\sigma_1$ . On the other hand,  
457 structures with low dip - still NW-SE oriented - could be attributed to previous compressive deformation phases linked to a  
458 stress field characterised by a horizontal  $\sigma_1$ , oriented NE-SW.

459 Taking into careful consideration the different depths investigated by the STAR boreholes ( $< 0.2$  km) with respect to the active  
460 stress data mainly inferred from breakout data in deep wells (0.5-6 km) and focal mechanisms of crustal earthquakes (usually  
461 5-15 km), we can still compare their results (Fig. 11). In fact, most of the results from literature on the orientation of the stress  
462 field have shown that different crustal depths do not reorient or change the stress field (Heidbach et al., 2016; Mariucci and  
463 Montone, 2024). An almost constant orientation of the minimum horizontal stress characterises this sector of the Apennines,  
464 from the southern L'Aquila and Norcia zones to the areas north of Gubbio, showing only a slight rotation from ENE-NE  
465 directions to NE-NNE directions, respectively (Fig. 11). This is observed from numerous data derived from earthquake focal  
466 mechanisms as well as breakout data in deep wells, also present in the southernmost sector (Mariucci and Montone, 2016) and  
467 active fault data (Lavecchia et al., 2022), under a stress regime that can be defined as exclusively extensional.

468 In conclusion, our paper provides reliable values on physical properties of rocks, in particular P-wave velocity, which can be  
469 used to characterise crustal velocity models and allow detailed interpretation of seismic profiles, investigating the first two  
470 hundred metres of the crust.



471 **References**

- 472 Amato, A. and Cocco, M. (eds): The Umbria-Marche, central Italy, Seismic Sequence of 1997–1998, *Journal of Seismology*,  
473 4(4), 5–598, 2000.
- 474 Amato, A., Azzara, R., Chiarabba, C., Cimini, G. B., Cocco, M., Di Bona, M., Margheriti, L., Mazza, S., Mele, F., Selvaggi, G.,  
475 Basili, A., Boschi, E., Courboux, F., Deschamps, A., Gaffet, S., Bittarelli, G., Chiaraluce, L., Piccinini, D., and Ripepe, M.:  
476 The 1997 Umbria-Marche seismic sequence: a first look at the main shocks and aftershocks, *Geophysical Research Letters*, 25,  
477 2861–2864, 1998.
- 478 Arthur, M. A. and Fischer, A. G.: Upper Cretaceous-Paleocene magnetic stratigraphy at Gubbio, Italy I. Lithostratigraphy and  
479 sedimentology, *Geological Society of American Bulletin*, 88, 367–371, 1977.
- 480 Barchi, M. R., De Feyter, A., Magnani, M.B., Minelli, G., Piali, G. and Sotera, B. M.: The structural style of the Umbria-Marche  
481 fold and thrust belt, *Memorie della Società Geologica Italiana*, 52, 557–578, 1998.
- 482 Barchi, M. R., Carboni, F., Michele, M., Ercoli, M., Giorgetti, C., Porreca, M., Azzaro, S., Chiaraluce, L.: The influence of  
483 subsurface geology on the distribution of earthquakes during the 2016-2017 Central Italy seismic sequence, *Tectonophysics*,  
484 807, 22879, <https://doi.org/10.1016/j.tecto.2021.228797>, 2021.
- 485 Barchi, M. R. and Collettini, C.: Seismicity of central Italy in the context of the geological history of the Umbria-Marche  
486 Apennines, *Special Paper of the Geological Society of America*, 542, 175 – 190, 2019.
- 487 Barchi, M. R. and Mirabella, F.: The 1997-98 Umbria-Marche earthquake sequence: "Geological" vs. "seismological" faults,  
488 *Tectonophysics*, 476(1-2), 170-179, [10.1016/j.tecto.2008.09.013](https://doi.org/10.1016/j.tecto.2008.09.013) (2009).
- 489 Barchi, M. R.: The Neogene-Quaternary evolution of the Northern Apennines: crustal structure, style of deformation and  
490 seismicity, *Journal of the Virtual Explorer*, 36, 2010.
- 491 Bigi, S., Casero, P., and Ciotoli, G.: Seismic interpretation of the Laga basin; constraints on the structural setting and kinematics  
492 of the Central Apennines, *Journal of Geological Society of London*, 168, 179–190, <https://doi.org/10.1144/0016-76492010-084>,  
493 2011.
- 494 Bohnhoff, M., Dresen, G., Ceken, U., Kadirioğlu, F. T., Kartal, R. F., Kilic, T., Nurlu, M., Yanik, K., Acarel, D., Bulut, F.,  
495 Kloth, A., Johnson, W., Malin, P. and Mencin, D.: GONAF – the borehole Geophysical Observatory at the North Anatolian  
496 Fault in the eastern Sea of Marmara, *Scientific Drilling: reports on deep earth sampling and monitoring*, 22, 19-28,  
497 <https://doi.org/10.5194/sd-22-19-2017>, 2017.
- 498 Boncio, P. and Lavecchia, G.: A geological model for the Colfiorito earthquakes (September–October 1997, central Italy),  
499 *Journal of Seismology*, 4, 345–356, 2000.
- 500 Boncio, P., Pizzi, A., Brozzetti, F., Pomposo, G. Lavecchia, G., Di Naccio, D., Ferrarini, F.: Coseismic ground deformation of  
501 the 6 April 2009 L'Aquila earthquake (central Italy, Mw6.3), *Geophysical Research Letters*, 37, L06308, 2010.



- 502 Caricchi, C., Aldega, L., Barchi, M. R., Corrado, S., Grigo, D., Mirabella, F., Zattin, M.: Exhumation patterns along shallow  
503 low-angle normal faults: an example from the Altotiberina active fault system (Northern Apennines, Italy), *Terra Nova*, 27, 312–  
504 321, <https://doi.org/doi:10.1111/ter.12163>, 2015.
- 505 Cello, G., Mazzoli, S., Tondi, E., and Turco, E.: Active tectonics in the central Apennines and possible implications for seismic  
506 hazard analysis in peninsular Italy, *Tectonophysics*, 272, 43–68, [http://dx.doi.org/10.1016/S0040-1951\(96\)00275-2](http://dx.doi.org/10.1016/S0040-1951(96)00275-2), 1997.
- 507 Chiarabba, C., De Gori, P., Cattaneo, M., Spallarossa, D., and Segou, M.: Faults geometry and the role of fluids in the 2016-  
508 2017 Central Italy seismic sequence, *Geophys. Res. Lett.*, 45, 6963–6971, <https://doi.org/10.1029/2018GL077485>, 2018.
- 509 Chiarabba, C., Jovane, L., and Di Stefano, R.: A new view of Italian seismicity using 20 years of instrumental recordings,  
510 *Tectonophysics*, 305, 251–268, 2005.
- 511 Chiaraluca, L., Di Stefano, R., Tinti, E., Scognamiglio, L., Michele, M., Casarotti, E., Cattaneo, M., De Gori, P., Chiarabba, C.,  
512 Monachesi, G., Lombardi, A., Valoroso, L., Latorre, D., Marzorati, S.: The 2016 Central Italy seismic sequence: a first look at  
513 the mainshocks, aftershocks, and source models, *Seismological Research Letters*, 88(3), 757–771,  
514 <https://doi.org/10.1785/0220160221>, 2017b.
- 515 Chiaraluca, L., Amato, A., Carannante, S., Castelli, V., Cattaneo, M., Cocco, M., Collettini, C., D’Alema, E., Di Stefano, R.,  
516 Latorre, D., Marzorati, S., Mirabella, F., Monachesi, G., Piccinini, D., Nardi, A., Piersanti, A., Stramondo, S., and Valoroso, L.:  
517 The Alto Tiberina Near Fault Observatory (northern Apennines, Italy), *Annals of Geophysics*, 57, S0327,  
518 <https://doi.org/10.4401/ag-6426>, 2014a.
- 519 Chiaraluca, L., Festa, G., Bernard, P., Caracausi, A., Carliccio, I., Clinton, J., Di Stefano, R., Elia, L., Evangelidis, C., Ergintav,  
520 S., Jianu, O., Kaviris, G., Marmureanu, A., Sebel, S., and Sokos, E.: The Near Fault Observatory community in Europe: a new  
521 resource for faulting and hazard studies, *Annals of Geophysics*, 65(3), <https://doi.org/10.4401/ag-8778>, 2022.
- 522 Chiaraluca, L., Festa, G., Bernard, P., Caracausi, A., Carluccio, I., Clinton, J.F., Di Stefano, R., Elia, L., Evangelidis, C.P.,  
523 Ergintav, S., Jianu, O., Kaviris, G., Marmureanu, A., Šebela, S., and Sokos, E.: The role of rheology, crustal structures and  
524 lithology in the seismicity distribution of the northern Apennines, *Tectonophysics*, 694, 280–291.  
525 <https://doi.org/10.1016/j.tecto.2016.11.011>, 2017a.
- 526 Chiaraluca, L., Collettini, C., Cattaneo, M., and Monachesi, G.: The shallow boreholes at the Altotiberina near fault Observatory  
527 (TABOO; northern Apennines of Italy), *Scientific Drilling*, 17, 31–35, <https://doi.org/10.5194/sd-17-31-2014>, 2014b.
- 528 Chiaraluca, L., Ellsworth, W. L., Chiarabba, C., and Cocco, M.: Imaging the complexity of an active normal fault system: The  
529 1997 Colfiorito (Central Italy) case study, *Journal of Geophysical Research*, 108(B6), <https://doi.org/10.1029/2002JB002166>,  
530 2003.
- 531 Chiaraluca, L., Mencin, D., Bennett, R., Barchi, M.R., Bohnhoff, M., and the STAR team: A strainmeter array to unravel the  
532 Alto Tiberina fault slip behaviour, Central Italy - ICDP STAR Drilling Project, EGU 2023-8462,  
533 <https://doi.org/10.5194/egusphere-egu23-8462>, 2023.





- 534 Ciaccio, M.G., Barchi, M.R., Chiarabba, C., Mirabella, F., and Stucchi, E.: Seismological, geological and geophysical constraints  
535 for the Gualdo Tadino fault, Umbria–Marche Apennines (central Italy), *Tectonophysics*, 406(3-4), 233-247,  
536 <https://doi.org/10.1016/j.tecto.2005.05.027> (2005).
- 537 Cinti, F. R., Cucci, L., Marra, F., and Montone, P.: The 1997 Umbria-Marche (Italy) earthquake sequence: Relationship between  
538 ground deformation and seismogenic structure, *Geophysical Research Letters*, 26, 895–898, 1999.
- 539 Collettini, C., Barchi, M. R., De Paola, N., Trippetta, F., and Tinti, E.: Rock and fault rheology explain differences between on  
540 fault and distributed seismicity, *Nature communication*, 13, 5627, <https://doi.org/10.1038/s41467-022-33373-y>, 2022.
- 541 Cresta, S., Monechi, S., and Parisi, G.: Stratigrafia del Mesozoico al Cenozoico nell’area Umbro-Marchigiana, *Memorie*  
542 *Descrittive della Carta Geologica d’Italia*, 34, 185, 1989.
- 543 Davatzes, N.C. and Hickman, S.H.: Stress, fracture, and fluid-flow analysis using acoustic and electrical image logs in hot  
544 fractured granites of the Coso geothermal field, California, U.S.A., in M. Poppelreiter, C. Garcia-Carballido, and M. Kraaijveld,  
545 eds., *Dipmeter and borehole image log technology*. AAPG Memoir 92, p. 259 – 293, 2010.
- 546 De Paola, N., Faulkner, D.R., and Collettini, C.: Localized versus distributed deformation as a control on the evolution of  
547 permeability in anhydrite rocks, *Journal of Geophysical Research*, 114, B06211, <http://dx.doi.org/10.1029/2008JB005967>, 2009.
- 548 Deschamps, A., Iannaccone, G., and Scarpa, R.: The Umbrian earthquake (Italy) of 19 September 1979, *Annales Geophysicae*,  
549 2(1), 29-36, 1984.
- 550 Diaferia, I., Barchi, M., Loddo, M., Schiavone, D., and Siniscalchi, A. Detailed imaging of tectonic structures by multiscale  
551 Earth resistivity tomographies: The Colfiorito normal faults (central Italy). *Geophys. Res. Lett.*, 33, L09305,  
552 [doi:10.1029/2006GL025828](https://doi.org/10.1029/2006GL025828), 2006
- 553 Ellis D.V. and Singer J.M.: *Well Logging for Earth Scientists*. 2nd edition Springer, pp 699, 2007.
- 554 EMERGEIO Working Group: Evidence for surface rupture associated with the Mw 6. 3 L’Aquila earthquake sequence of April  
555 2009 (central Italy), *Terra Nova*, 22, 43–51, 2010.
- 556 Fischer, T., Hrubcová, P., Dahm, T., Woith, H., Vylita, T., Ohrnberger, M., Vlček, J., Horálek, J., Dedeček, P., Zimmer, M.,  
557 Lipus, M., Pierdominici, S., Kallmeyer, J., Krüger, F., Hannemann, K., Korn, M., Kämpf, H., Reinsch, T., Klicpera, J., Volmer,  
558 D., Daskalopoulou, K. (2022). ICDP Eger Rift observatory: Magmatic Fluids Driving the Earthquake Swarms and Deep  
559 Biosphere - Scientific and technological achievements, *Scientific Drilling*, 31, 31-49, <https://doi.org/10.5194/sd-31-31-2022>
- 560 Haessler, H., Gaulon, R., Rivera, L., Console, R., Frogneux, M., Gasparini, G., Martel, L., Patau, G., Siciliano, M., and Cisternas,  
561 A.: The Perugia (Italy) earthquake of 29 April 1984: a microearthquake survey, *Bulletin of the Seismological Society of America*,  
562 78, 1948–1964, 1988.
- 563 Hairabian, A., Fournier, F., Borgomano, J., and Nardon, S.: Depositional facies, pore types and elastic properties of deep-water  
564 gravity flow carbonates *Journal of Petroleum Geology*, 37, 231–249, 2014.
- 565 Heidbach, O., Rajabi, M., Reiter, K., Ziegler, M., and WSM Team: World Stress Map Database Release 2016. V. 1.1, GFZ Data  
566 Services, <https://doi.org/10.5880/WSM.2016.001>, 2016.



- 567 Italian CMT dataset (<http://www.bo.ingv.it/RCMT/Italydataset.html>)
- 568 Langbein, J., Murray, J.R., and Snyder, H.A.: Coseismic and initial postseismic deformation from the 2004 Parkfield, California,  
569 earthquake, observed by Global Positioning System, electronic distance meter, creepmeters, and borehole strainmeters, *Bulletin*  
570 *of the Seismological Society of America*, 96(4B), S304-S320, 2006.
- 571 Latorre, D., Mirabella, F., Chiaraluca, L., Trippetta, F., and Lomay, A.: Assessment of earthquake locations in 3-D deterministic  
572 velocity models: A case study from the Altotiberina Near Fault Observatory (Italy), *Journal of Geophysical Research: Solid*  
573 *Earth*, 121(11), 8113-8135, <https://doi.org/10.1002/2016JB013170>, 2016.
- 574 Lavecchia, G., Adinolfi, G. M., de Nardis, R., Ferrarini, F., Cirillo, D., Brozzetti, F., De Matteis, R., Festa, G., and Zollo, A.:  
575 Multidisciplinary inferences on a newly recognized active east-dipping extensional system in Central Italy, *Terra Nova*, 29, 77–  
576 89, 2017.
- 577 Lavecchia, G., Bello, S., Andrenacci, C., Cirillo, D., Ferrarini, F., Vicentini, N., de Nardis, R., Roberts, G., Brozzetti, F.:  
578 Quaternary fault strain INDicators database - QUIN 1.0-first release from the Apennines of central Italy, *Scientific Data*, 9(1),  
579 doi 10.1038/s41597-022-01311-8, 2022.
- 580 Mariucci M.T. and Montone P.: Contemporary stress field in the area of the 2016 Amatrice seismic sequence (central Italy),  
581 *Annals of Geophysics*, 59, fast track 5, doi:10.4401/ag-7235, 2016.
- 582 Mariucci M.T., Montone P., and Pierdominici S.: Active stress field in central Italy: a revision of deep well data in Umbria  
583 region, *Annals of Geophysics*, 51, 2/3, 433-442, 2008.
- 584 Mariucci, M.T. and Montone, P.: IPSI 1.6, Database of Italian Present-day Stress Indicators, Istituto Nazionale di Geofisica e  
585 Vulcanologia (INGV), <http://doi.org/10.13127/IPSI.1.6>, 2024.
- 586 Marzorati, S., Massa, M., Cattaneo, M., Monachesi, G., and Frapiccini, M.: Very detailed seismic pattern and migration inferred  
587 from the April 2010 Pietralunga (northern Italian Apennines) micro-earthquake sequence, *Tectonophysics*, 610, 91–109,  
588 <https://doi.org/10.1016/j.tecto.2013.10.014>, 2014.
- 589 Massiot, C., McNamara, D., and Lewis, B.: Processing and analysis of high temperature geothermal acoustic borehole image  
590 logs in the Taupo Volcanic Zone, New Zealand, *Geothermics*, 53, 190–201, <https://doi.org/10.1016/j.geothermics.2014.05.010>,  
591 2015.
- 592 Michele, M., Chiaraluca, L., Di Stefano, R., and Waldhauser, F.: Fine-Scale Structure of the 2016–2017 Central Italy Seismic  
593 Sequence From Data Recorded at the Italian National Network, *Journal of Geophysical Research*, 125, e2019JB01844,  
594 <https://doi.org/10.1029/2019JB018440>, 2020.
- 595 Mildon, Z. K., Roberts, G. P., Faure Walker, J. P., Wedmore, L. N. J., and McCaffrey, K. J. W.: Active normal faulting during  
596 the 1997 seismic sequence in Colfiorito, Umbria: Did slip propagate to the surface?, *Journal of Structural Geology*, 91, 102–  
597 113, 2016.
- 598 Mirabella, F., Brozzetti, F., Lupattelli, A., and Barchi, M.R.: Tectonic evolution of a low-angle extensional fault system from  
599 restored cross-sections in the Northern Apennines (Italy), *Tectonics*, 30, TC6002, doi:10.1029/2011TC002890, 2011.



- 600 Mirabella, F., Ciaccio, M.G., Barchi, M.R., and Merlini, S.: The Gubbio normal fault (Central Italy): geometry, displacement  
601 distribution and tectonic evolution, *Journal of Structural Geology*, 26, 2233-2249, doi:10.1016/j.jsg.2004.06.009, 2004.
- 602 Montone, P. and Mariucci, M. T.: The new release of the Italian contemporary stress map, *Geophysical Journal International*,  
603 205, 1525–1531, <https://doi.org/10.1093/gji/ggw100>, 2016.
- 604 Montone, P. and Mariucci, M.T.: Constraints on the Structure of the Shallow Crust in Central Italy from Geophysical Log Data,  
605 *Scientific Reports*, 10, 3834, <https://doi.org/10.1038/s41598-020-60855-0>, 2020.
- 606 Montone, P. and Mariucci M.T.: Lateral Variations of P-Wave Velocity from Deep Borehole Data in the Southern Apennines,  
607 Italy, *Pure and Applied Geophysics*, 180, 1925–1944, <https://doi.org/10.1007/s00024-023-03248-4>, 2023.
- 608 Pierdominici, S. and Kück, J.: Borehole Geophysics. In: *Encyclopedia of Geology (Second Edition)*, Elsevier, 746-760,  
609 <https://doi.org/10.1016/B978-0-08-102908-4.00126-0>, 2021.
- 610 Pierdominici, S., Millett, J. M., Kück, J. K. M., Thomas, D., Jerram, D. A., Planke, S., Haskins, E., Lautze, N., and Galland, O.:  
611 Stress field interactions between overlapping shield volcanoes: Borehole breakout evidence from the island of Hawaii, USA,  
612 *Journal of Geophysical Research*, 125, e2020JB019768, <https://doi.org/10.1029/2020JB019768>, 2020.
- 613 Pizzi, A., Di Domenica, A., Gallovic, F., Luzi, L., and Puglia, R.: Fault segmentation as constraint to the occurrence of the main  
614 shocks of the 2016 Central Italy seismic sequence, *Tectonics*, 36, 2370–2387, <https://doi.org/10.1002/2017TC004652>, 2017.
- 615 Pondrelli, S. and Salimbeni, S.: Italian CMT Dataset (Data set). Istituto Nazionale di Geofisica e Vulcanologia (INGV),  
616 <https://doi.org/10.13127/rcmt/italy>, 2006.
- 617 Pondrelli, S., Salimbeni, S., Ekström, G., Morelli, A., Gasperini, P., and Vannucci, G.: The Italian CMT dataset from 1977 to  
618 the present, *Physics of the Earth and Planetary Interiors*, 159(3-4), 286-303, doi:10.1016/j.pepi.2006.07.008, 2006.
- 619 Porreca, M., Minelli, G., Ercoli, M., Brobia, A., Mancinelli, P., Cruciani, F., Giorgetti, C., Carboni, F., Mirabella, F., Cavinato,  
620 G., Cannata, A., Pauselli, C., and Barchi, M. R.: Seismic reflection profiles and subsurface geology of the area interested by the  
621 2016–2017 earthquake sequence (Central Italy), *Tectonics*, 37, 1116–1137, <https://doi.org/10.1002/2017TC004915>, 2018.
- 622 Price, N.J. *Fault and Joint Development in Brittle and Semi-Brittle Rocks*. Pergamon Press, Oxford, 1966 Quick Regional  
623 Moment Tensors, <http://autorcmt.bo.ingv.it/quicks.html>
- 624 Rider, M.H. and Kennedy, M.: *The Geological Interpretation of Well Logs*, 432 pp, Rider-French, Scotland, 2011.
- 625 Schön, J.H.: *Physical Properties of Rocks - Fundamentals and Principles of Petrophysics*. 2nd Edition -Elsevier, 2015.
- 626 Scisciani, V., Agostini, S., Calamita, F., Pace, P., Cilli, A., Giori, I., and Paltrinieri, W.: Positive inversion tectonics in foreland  
627 fold-and thrust belts: a reappraisal of the Umbria–Marche northern Apennines (Central Italy) by integrating geological and  
628 geophysical data, *Tectonophysics*, 637, 218–237, <https://doi.org/10.1016/j.tecto.2014.10.010>, 2014.
- 629 Serra, O.: *Fundamentals of well-log interpretation. Part 1: The acquisition of logging data*. Developments in petroleum science  
630 15A, Amsterdam, Elsevier, pp 435, 1984.
- 631 Smeraglia, L., Trippetta, F., Carminati, E., and Mollo, S.: Tectonic control on the petrophysical properties of foredeep sandstone  
632 in the Central Apennines, Italy, *Journal of Geophysical Research*, 119, 9077–9094, 2014.



- 633 Terzaghi, R. D.: Sources of error in joint surveys, *Geotechnique*, 15(3), 287–304, <https://doi.org/10.1680/geot.1965.15.3.287>,  
634 1965.
- 635 Tinti, E., Scognamiglio, L., Michelini, A., and Cocco, M.: Slip heterogeneity and directivity of the ML 6.0 2016 Amatrice  
636 earthquake estimated with rapid finite-fault inversion, *Geophysical Research Letters*, 43(10), 10,745–10,752,  
637 <https://doi.org/10.1002/2016GL071263>, 2016.
- 638 Trippetta F., Barchi, M. R., Tinti, E., Volpe, G., Rosset, G., and De Paola, N.: Lithological and stress anisotropy control  
639 large-scale seismic velocity variations in tight carbonates, *Scientific Reports*, 11, 9472, [https://doi.org/10.1038/s41598-021-  
640 89019-4](https://doi.org/10.1038/s41598-021-89019-4), 2021.
- 641 Trippetta, F., Collettini, C., Vinciguerra, S., and Meredith, P.G.: Laboratory measurements of the physical properties of Triassic  
642 evaporites from central Italy and correlation with geophysical data, *Tectonophysics*, 492, 121–132,  
643 <http://dx.doi.org/10.1016/j.tecto.2010.06.001>, 2010.
- 644 Valoroso, L., Chiaraluce, L., Di Stefano, R., and Monachesi, G.: Mixed-mode slip behaviour of the Altotiberina low-angle  
645 normal fault system (Northern Apennines, Italy) through high-resolution earthquake locations and repeating events, *Journal of  
646 Geophysical Research: Solid Earth*, 122, <https://doi.org/10.1002/2017JB014607>, 2017.
- 647 Valoroso, L., Chiaraluce, L., Piccinini, D., Di Stefano, R., and Waldhauser, F.: Radiography of a normal fault system by 64,000  
648 high-precision earthquake locations: The 2009 L'Aquila (central Italy) case study, *Journal of Geophysical Research: Solid Earth*,  
649 118, 1156-1176, <https://doi.org/10.1002/jgrb.50130>, 2013.
- 650 Villani, F., Civico, R., Pucci, S., Pizzimenti, L., Nappi, R., De Martini, P. M., and the Open EMERGEIO Working Group: A  
651 database of the coseismic effects following the 30 October 2016 Norcia earthquake in Central Italy, *Scientific Data*, 5, 180049,  
652 <https://doi.org/10.1038/sdata.2018.49>, 2018.

653

## 654 **Data Availability**

655 After a 3-year embargo period, starting from the end of drilling the last hole (TMS06 summer 2022), the  
656 downhole logging dataset will be available at the ICDP repository database ([https://www.icdp-  
657 online.org/projects/by-continent/europe/star-italy/internal-data](https://www.icdp-online.org/projects/by-continent/europe/star-italy/internal-data)). Currently, the dataset is not available  
658 for public download. Who is interested should contact the principal investigator of the ICDP STAR  
659 project (Lauro Chiaraluce [lauro.chiaraluce@ingv.it](mailto:lauro.chiaraluce@ingv.it)).

## 660 **Author Contributions**

661 Author Contributions: PM, SP, MRB conceptualization, methodology; PM, SP, MTM, AA formal  
662 analysis; PM, SP, MTM, LC, MU, FM, WJ field investigation; LC, AA, MU, FM data curation; PM,  
663 SP, MRB, MTM writing—original draft preparation; SP, MU, MTM visualisation; PM, SP, MRB,



664 MTM writing—review and editing. All co-authors contributed to reviewing and revising the paper. All  
665 authors have read and agreed to the published version of the manuscript.

### 666 **Competing Interests**

667 The authors declare that they have no conflict of interests.

### 668 **Acknowledgments**

669 GEOTEC (<http://geo-tec.it/en/>) and GEOLOGIN Srl (<https://www.geolog-in.com/>) are thanked for  
670 providing drillings and geophysical borehole log data. We are grateful to Earthscope for providing  
671 strainmeters. STAR drilling project is co-funded by the International Continental Scientific Drilling  
672 Program (ICDP), by the United States National Science Foundation (NSF) and by the Italian Istituto  
673 Nazionale di Geofisica e Vulcanologia (INGV).

674

### 675 **Supplementary Material**

676 See Supplementary file